Diversity of MJO Initiation Regions and Processes

TIANYI WANG[a,b] AND TIM LI[a,b,c]

[a] *Key Laboratory of Meteorological Disaster, Ministry of Education/Joint International Research Laboratory of Climate and Environmental Change/Collaborative Innovation Center on Forecast and Evaluation of Meteorological Disasters, Nanjing University of Information Science and Technology, Nanjing, China*
[b] *International Pacific Research Center, School of Ocean and Earth Science and Technology, University of Hawai'i at Mānoa, Honolulu, Hawaii*
[c] *Department of Atmospheric Sciences, School of Ocean and Earth Science and Technology, University of Hawai'i at Mānoa, Honolulu, Hawaii*

(Manuscript received 21 October 2021, in final form 19 June 2022)

ABSTRACT: The diversity of the Madden–Julian oscillation (MJO) initiation (i.e., initial onset of active convection before moving eastward) regions was explored using a clustering method. Regions favorable for MJO initiations are grouped into four longitude zones: the Atlantic and Africa (AA), the Indian Ocean (IO), the Maritime Continent (MC), and the western Pacific (WP). The region-dependent dominant initiation mechanisms are explored using a composite procedure. The AA initiation is attributed to a circumnavigating process associated with a preceding MJO. As upper-tropospheric westerly anomalies move into the AA region, the associated descending motion leads to suppressed convection over the IO, which further triggers convection onset to its west through anomalous westward moisture advection. The IO initiation arises from the downstream forcing of a preceding suppressed phase of MJO. A delayed air–sea interaction process also plays a role. The MC initiation is triggered by a westward-propagating dry equatorial Rossby wave in the Pacific. The low-level poleward flows associated with the anticyclonic Rossby wave gyres advect high mean moisture, promoting the convection onset over the MC. The WP initiation is triggered by a preceding suppressed phase of MJO that moves eastward, in a way similar to the downstream scenario in the IO. The AA initiation is usually associated with a La Niña–like background sea surface temperature pattern, which favors the decoupling of upper-tropospheric westerly anomalies from the preceding MJO. The MC and WP initiations are more frequent during El Niño, as the relevant meridional moisture gradient is sharper and the eastern Pacific is moister.

KEYWORDS: Madden-Julian oscillation; Intraseasonal variability; Tropical variability; El Niño; La Niña

1. Introduction

The earliest known publication to identify, and recognize the synoptic impacts of, what subsequently came to be known as the tropical intraseasonal oscillation dates back to Xie et al. (1963) [see a report by Li et al. (2018)]. Madden and Julian (1971, 1972) identified a planetary-scale eastward-propagating mode across the whole tropics with a period of 40–50 days, which is now named as the Madden–Julian oscillation (MJO). The MJO, as the dominant mode of tropical intraseasonal variability, was confirmed by further studies with the help of satellite data. Its broadband feature (spans a range of 20–100 days), complexity in origins and propagations, and pronounced seasonality are also unveiled [see reviews by Madden and Julian (1994) and Zhang (2005)]. Given its intraseasonal time scale and slowly propagating nature, the MJO serves as a cornerstone in the subseasonal-to-seasonal (S2S) prediction that bridges the weather and climate (Zhang 2013; Vitart et al. 2017).

The MJO typically initiates over the Indian Ocean and propagates eastward (Straub 2013). However, current MJO research has found much diversity. A recent work by Wang et al. (2019) unveiled the diversity of MJO in terms of its propagating features with the help of an objective clustering method. By using similar clustering methods, a series of studies on the MJO diversities relevant to various aspects have been conducted, such as the propagation and intensity (Wang and Li 2021), teleconnections (Chen 2021), and seasonal (Chen and Wang 2021) and spatial (Wang et al. 2021) dependence.

The initiation of the MJO, which refers to the initial onset of active convection before it moves eastward, has a very different mechanism from the propagation, and is still an open and challenging topic [see Li (2014) and Li et al. (2020) for recent reviews on this issue]. A widely accepted hypothesis is the so-called circumnavigating theory (e.g., Lau and Peng 1987; Knutson and Weickmann 1987; Hendon 1988; Wang and Li 1994; Matthews 2000, 2008). The promise behind is that the equatorial atmospheric waves associated with a preceding MJO travel around the global tropics and may trigger deep convection over the relatively moist and warm Indian Ocean. These MJO events are referred to as a "successive" MJO event since it follows an immediately preceding one (Matthews 2008). Specific processes related to the convection onset may include the adiabatic lifting due to the upper-tropospheric divergent

Supplemental information related to this paper is available at the Journals Online website: https://doi.org/10.1175/JCLI-D-21-0816.s1.

Dr. Wang's current affiliation is School of Marine Science and Technology, Zhejiang Ocean University, Zhoushan, China

Corresponding author: Tim Li, timli@hawaii.edu

DOI: 10.1175/JCLI-D-21-0816.1

perturbation (Matthews 2008; Powell and Houze 2015; Haertel et al. 2015; Powell 2016), low-level moisture convergence (Seo and Kim 2003; Kikuchi and Takayabu 2003; Chen and Zhang 2019), and topographic lifting effects (Hsu and Lee 2005), among others. In the scenario of circumnavigation, the forcing from upstream (west of the MJO initiation region) holds the key to MJO initiation.

The circumnavigating theory, however, has been deemed not crucial for MJO initiation over the western Indian Ocean by idealized numerical model experiments (Zhao et al. 2013; Ray and Li 2013; Maloney and Wolding 2015) and observational analyses (Zhao et al. 2013; Mei et al. 2015; Li et al. 2015; Nasuno et al. 2015). Different from the upstream forcing scenario, Zhao et al. (2013) proposed a downstream forcing scenario relevant to successive MJO events. That is, a preceding convectively suppressed phase of MJO may trigger new active MJO convection over the western Indian Ocean, after it moves to eastern Indian Ocean. The MJO convection onset is mainly through the westward advection of background moisture by the low-level easterly anomaly. The latter is a result of the equatorial Rossby (ER) wave response to the preceding convectively suppressed phase of MJO.

Besides the upstream and downstream mechanisms, other studies suggested a "discharge–recharge" paradigm that emphasizes local processes such as surface fluxes, cloud–radiation feedbacks, sea surface temperature (SST), and boundary layer moisture convergence (e.g., Bladé and Hartmann 1993; Hu and Randall 1994; Kemball-Cook and Weare 2001; Jiang and Li 2005; Benedict and Randall 2007; Li et al. 2008; Sobel et al. 2014; Rydbeck and Jensen 2017). Interactions of equatorial waves and mean circulation have also been addressed (e.g., Feng and Li 2016; Takasuka et al. 2021; Kohyama et al. 2021). For instance, given that the southern Indian Ocean has a strong intraseasonal SST variability during boreal winter when the climatological mean thermocline is shallow (Li et al. 2002; Saji et al. 2006), Li et al. (2008) proposed a delayed air–sea interaction mechanism in which a preceding active MJO convection could trigger a suppressed phase of MJO through a delayed effect of cold SST wake.

In addition to the tropical origins described above, the extratropical processes such as midlatitude perturbations propagating into the tropics also play a role in the MJO initiation (e.g., Hsu et al. 1990; Kiladis and Weickmann 1992; Matthews and Kiladis 1999; Pan and Li 2008; Ray et al. 2009; Ray and Li 2013; Roundy 2014), which is possibly more applicable to "primary" events. For example, a case study by Hsu et al. (1990) suggested a midlatitude wave source from the Northern Hemisphere. On the other hand, Zhao et al. (2013) pointed out that the Southern Hemisphere Rossby wave forcing is more crucial based on their idealized numerical model experiments.

While most previous studies focus on the Indian Ocean which is the most frequent region of MJO initiation (Wang and Rui 1990; Zhang and Ling 2017), the MJO initiation is not limited to this area. In an early study, Wang and Rui (1990) analyzed the paths of tropical intraseasonal convection anomalies (TICA) case by case and found that although it is maximized over the western Indian Ocean, the geographic distribution of TICA initiations spans a large area from tropical Atlantic, Africa to eastern Indian Ocean. Perhaps because a longer data period is used, Matthews (2008) further identified MJO initiations over the Maritime Continent and western Pacific, which was not reported in Wang and Rui (1990). These observationally based results suggest an explicit diversity of the MJO initiation regions. The initiation mechanisms and the associated precursory signals might also be region dependent.

Nevertheless, how the MJOs are initiated over the regions other than the Indian Ocean is a less studied topic. Also, it is unclear whether the existing hypotheses about the Indian Ocean MJO initiation are applicable to the other regions. Recently, Takasuka and Satoh (2021) systematically explored the MJO initiations over the Indian Ocean, Maritime Continent, and western Pacific. However, those three regions are subjectively determined in advance, not an objective classification. The Atlantic and Africa, which were previously identified in observations, are not included in their study. Besides, their work emphasized the role of interannual background in modulating the favorable initiation region, but the initiation mechanism itself is controversial. For instance, in their Indian Ocean and Maritime Continent scenarios, a basic premise is that the background state supports a local enhancement of intraseasonal convection that causes a suppressed convection anomaly to the west, the circulation of the latter advects moisture to the west and triggers a new convection there. However, the suppressed convection anomaly is more like an eastward-propagating suppressed phase of MJO (their Fig. 2a), which agrees with the downstream forcing scenario proposed by Zhao et al. (2013). It also seems odd that the amplification of this intraseasonal suppressed convection anomaly collocates with the suppressed background convection (their Fig. 10b), since a reduced background diabatic heating indicates a weak circulation–convection–moisture feedback which restrains the development of an anomalous descent (Wu et al. 2009; Wang and Li 2021).

In the current study we aim to further understand the diversity of the MJO initiation, with a particular focus on the classification of initiation regions and associated initiation mechanisms. For the former, we applied an objective cluster analysis to the MJO initiations around the global tropics, but not a few regions subjectively determined in advance. The initiation regions here actually refer to several equatorial longitude zones since they are identified in the Hovmöller diagrams (see section 3 for detail). For the latter, a lead–lag composite analysis is used to explore the precursory signals and processes associated with the MJO initiation. In particular, we placed focus on the moistening process that predominantly contributes to the convection onset. The composite procedure provides a knowledge of which dominant processes may contribute to the initiation over a given region, through analyzing the statistically significant signals. However, those unimportant or infrequent processes that cannot be statistically significantly distinguished from background noises in the composite are excluded. In addition, the climatological relative contribution of each dominant process requires a case-by-case study, which is beyond our scope.

The rest of the paper is organized as follows. Section 2 introduces the data and methods. Section 3 describes how the MJO initiations are identified and the diversity of initiation regions unveiled by the objective clustering method. Section 4 explores the precursory signals and processes associated with the MJO initiation over each region. A summary and discussion are given in section 5.

2. Data and methods

a. Data and preprocessing

The datasets used in this study include (i) the observed daily outgoing longwave radiation (OLR) from the National Oceanic and Atmospheric Administration (NOAA) (Liebmann and Smith 1996); (ii) the CPC Merged Analysis of Precipitation (CMAP) (Xie and Arkin 1997); (iii) the ERA5 reanalysis from the European Centre for Medium-Range Weather Forecasts (Hersbach et al. 2020); and (iv) the Group for High Resolution Sea Surface Temperature (GHRSST) Level 4 AVHRR_OI Global Blended Sea Surface Temperature Analysis (GDS2) from NCEI, version 2.1 (Reynolds et al. 2007). The OLR and CMAP datasets have a 2.5° × 2.5° spatial resolution. The raw ERA5 reanalysis is available at hourly with a 0.25° × 0.25° spatial resolution, and has been preprocessed to daily and 2.5° × 2.5° by using temporal and area averaging. This reduction in resolution makes the ERA5 data compatible with the observational OLR and CMAP datasets. It might also make the variables more coherent with tropical convective activities (Suematsu and Miura 2018). The sea surface temperature (SST) data are daily at a 0.25° × 0.25° spatial resolution. The period of boreal winters from 1979/80 to 2018/19 (from November to April) is used in the research.

The slow climatological annual cycle (annual mean and first three harmonics of climatological annual variation) of 1981–2010 has been removed to obtain the anomalous components. To extract the MJO-scale intraseasonal anomalies, a 20–80-day filter has been applied to the variables used in the lead–lag composite analysis. In addition, only the eastward-propagating components with zonal wavenumbers 1–9 of the intraseasonal OLR anomalies are retained when identifying the MJO events. The low-frequency background components are obtained by applying an 80-day low-pass filter to the raw anomalies. The temporal and spatial–temporal filtering are based on one-dimensional and two-dimensional Fourier harmonic analyses, respectively. A detailed description of the MJO events identification and the cluster analysis will be given in section 3. The composite procedure will be described at the beginning of section 4.

b. Moisture budget diagnosis

A low-level (1000–500 hPa) moisture budget diagnosis is applied in exploring the precursory signals and processes associated with the MJO initiation. First, a variable is decomposed into three different time scales:

$$X = \overline{X} + X' + X^*, \tag{1}$$

where X represents any time-dependent variable, and is decomposed into a low-frequency background component (>80 day, denoted by an overbar), an intraseasonal component (20–80 day, denoted by a prime), and a high-frequency component (<20 day, denoted by an asterisk). Then, the low-level moisture budget equation on the intraseasonal time scale is written as follows:

$$\langle \partial_t q \rangle' = -\langle u \partial_x q \rangle' - \langle v \partial_y q \rangle' + Q_C', \tag{2}$$

where q is the specific humidity; and u and v are the zonal and meridional velocities. The angle brackets represent a mass-weighted vertical integration from 1000 to 500 hPa. Following Chikira (2014) and Wolding and Maloney (2015), the vertical moisture advection and the residual term (known as the apparent moisture sink, Yanai et al. 1973) are combined as the "column process" Q_c.

We also diagnosed the surface upward water vapor flux (WVF) and the relative contribution by the intraseasonal SST anomaly to explore the possible role of air–sea interaction in the MJO initiation. The WVF can be empirically resolved by a bulk formula:

$$\mathrm{WVF} = \rho c_e U \Delta q, \tag{3}$$

where ρ is the air density, c_e is the turbulent exchange coefficient, U is the wind speed at 10 m above the sea surface, and Δq is the specific humidity difference between sea surface air and air at 2 m above. The surface specific humidity is computed from the saturation humidity for pure water at the respective SST, multiplied by a factor of 0.98 to fix the effect of typical salinity (Yu 2007; Yu et al. 2008). Therefore, SST change directly modulates the WVF by influencing Δq, and the WVF change contributed by the intraseasonal SST anomaly is approximately calculated as follows:

$$\mathrm{WVF}'_{\mathrm{sst}} = \overline{(\rho c_e)}\,\overline{U}\,\Delta q'. \tag{4}$$

Namely, the intraseasonal WVF anomaly caused by the intraseasonal SST perturbation is mainly attributed to the Δq change, where the other terms are treated as climatological. For a detailed procedure, readers are referred to the appendix A of Wang et al. (2018).

For convenience, we adopt the ERA5 reanalysis, which provided all necessary variables to calculate Eqs. (3) and (4). In a recent study (Pokhrel et al. 2020), the net heat flux and its components in four reanalysis (including ERA5) and two blended products are compared with in situ observations (including daily time series from two buoys located in tropical Indian Ocean). ERA5 performs best among all other products, which gives us confidence of applying the ERA5 products to estimate the WVF and its intraseasonal components. However, it is worth pointing out that uncertainties might exist in both the reanalysis and the bulk method.

3. Cluster analysis for MJO initiation regions

a. Identification of MJO initiation region

The MJO initiation has been reported in various locations of the tropics, and the diversity of which is to be concerned in

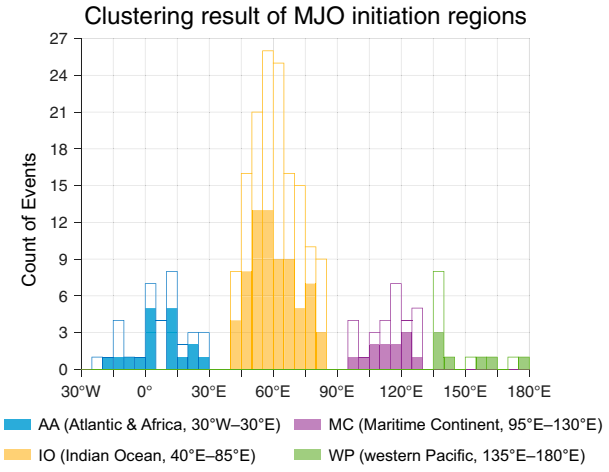

FIG. 1. Clustering result of the MJO initiation regions. Bars indicate count of MJO events initiated in each longitude bin during boreal winters from 1979/80 to 2018/19 (from November to April). A solid bar counts the events of active convection only, and a hollow bar include both convectively active and suppressed events. The longitude bin width of each bar is 5°.

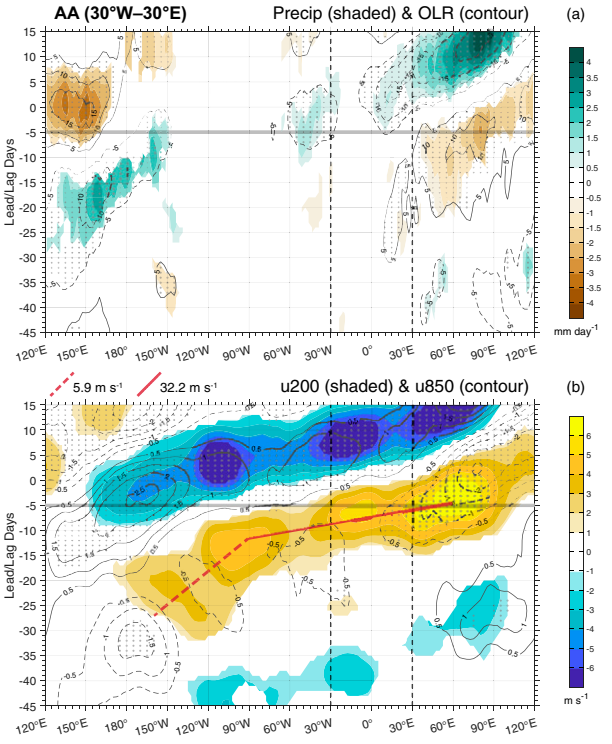

FIG. 2. Longitude–lead/lag time diagrams of composite intraseasonal anomalies averaged over 15°S–10°N of (a) precipitation (shaded) and OLR (contours; 5 W m^{-2} interval with zero omitted); and (b) zonal wind at 200 hPa (shaded) and 850 hPa (contours; 0.5 m s^{-1} interval with zero omitted), for the MJO wet events initiated over the AA region. Red dashed and solid lines in (b) are used for estimating the eastward speed of 200-hPa zonal wind before and after decoupling from the convection, respectively. In this and subsequent figures showing spatial (or spatial–temporal) sections of composite intraseasonal anomalies, the shading, stippling (for contours, if existing), and vectors (if existing) indicate statistically significant signals based on the FDR approach with $\alpha_{FDR} = 0.15$. Vertical thick dashed gray lines denote the longitude zone of the initiation region. In a longitude–lead/lag time diagram, day 25 is highlighted by a thick solid gray line, which roughly indicates the moment when organized eastward propagation of significant OLR anomalies begins.

this work. Therefore, Hovmöller diagrams across the full longitude domain should be examined in order to capture all possible initiation regions. Following Wang and Li (2021), the OLR field is first subjected to a spatial–temporal filtering to retain the period of 20–80 days and an eastward-propagating component with zonal wavenumbers 1–9, so as to extract MJO-scale signals in spatial and temporal domains (Kiladis et al. 2014). The so-calculated OLR anomalies are then averaged between 15°S and 10°N by taking into consideration of the slight southward shift of the MJO paths during boreal winter (Wang and Rui 1990; Zhao et al. 2013; Kim et al. 2017), and then are plotted in the Hovmöller diagrams. To get smooth contours and more precise initiation longitudes, the Hovmöller diagrams are first interpolated to 1° resolution in zonal direction, then the OLR anomalies are smoothed by a 5-day and 5° longitude running mean moving window. The contours of −10 and 10 W m^{-2} (about one standard deviation of the smoothed Hovmöller diagram averaged along the zonal direction) are selected as criteria for convectively enhanced and suppressed phases of MJO (in other words, "wet" and "dry" events), respectively. Additional criteria are that an MJO event must have a life span longer than 15 days and a propagation length greater than 45° in longitude over the warm pool region (55°E–140°W). These criteria ensure that all the selected events have an intraseasonal temporal scale, a planetary spatial scale, and a life cycle that is mainly active over the warm oceans. In total, 115 wet events and 119 dry events are picked up from 1979/80 to 2018/19 boreal winters, roughly 3 events each in a winter (6 months from November to April).

Although not all the events identified are initiated over the Indian Ocean as "classical" MJOs, the above criteria capture the most essential features relevant to the MJO definitions (Zhang 2005; Waliser et al. 2012; Wang et al. 2016; Wang and Chen 2017). Namely, an MJO is a large-scale slowly eastward-propagating (~5 m s^{-1}; see Fig. S1 in the online supplemental material for a histogram) intraseasonal convective system along the equator with most of its life cycle over the warm oceans (Fig. S2 shows Hovmöller diagrams of some individual cases).

To determine the initiation longitude and date, we adopted a tracking method proposed by Zhang and Ling (2017). For an MJO event identified in the Hovmöller diagram, we use the centroid of the contour to determine the reference longitude [not the fixed 90°E in the original procedure of Zhang and Ling (2017)]. Then, we run a set of straight lines passing the reference longitude at a given day inside the contour, each with its own slope. The line segment inside the contour with the largest OLR amplitude integrated along it is chosen as the optimum path. The initiation longitude and date are

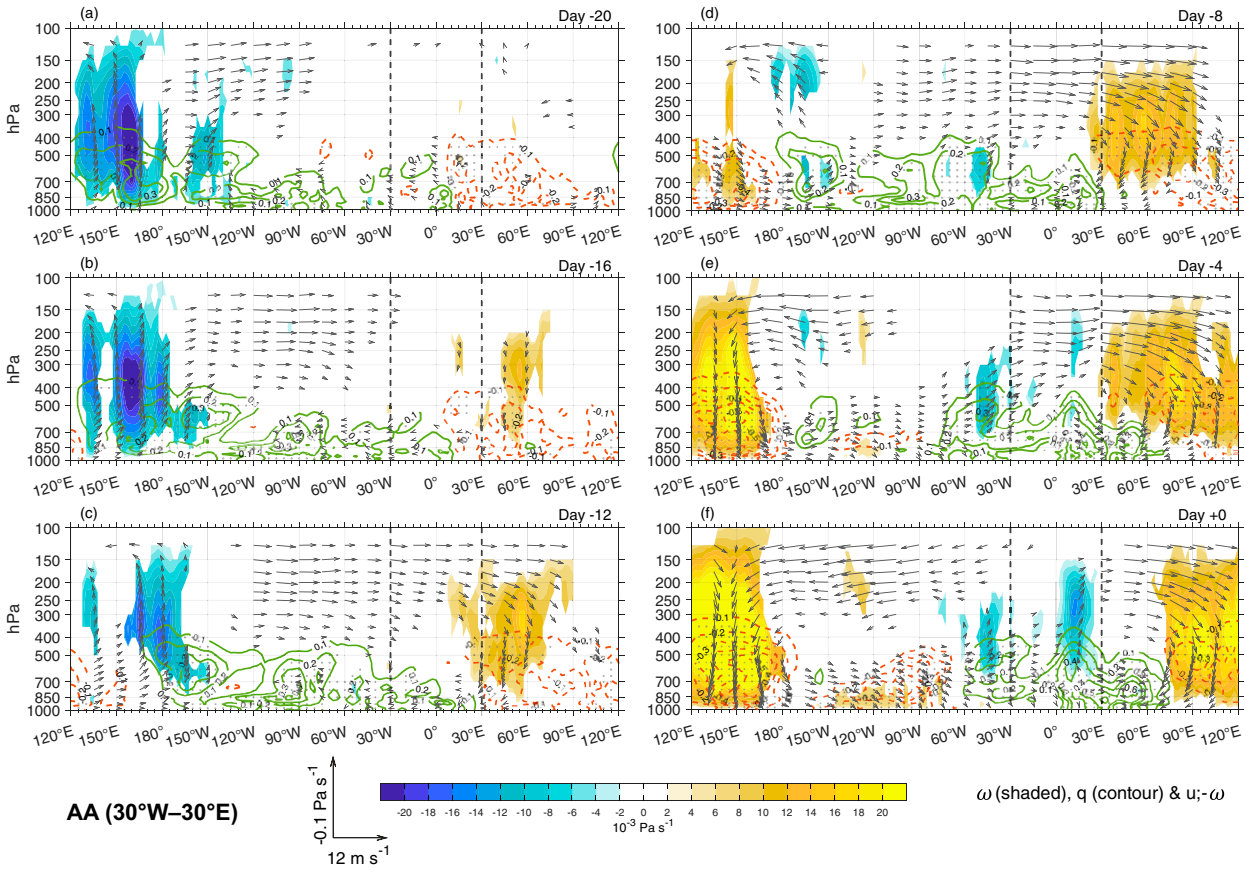

FIG. 3. Longitude–height diagrams of composite intraseasonal anomalies averaged over 15°S–10°N of vertical pressure velocity (shaded), specific humidity (contours; 0.1 g kg^{-1} interval with zero omitted, green solid for positive and red dashed for negative values), and vertically overturning circulation (vectors), for the MJO wet events initiated over the AA region.

simply identified according to the coordinate of the beginning point of the line segment of the optimum path.

It is worth pointing out that the initiation date identified with the above method does not necessarily represent the day that OLR anomaly transits from positive to negative, which is what is used in many previous studies (e.g., Zhao et al. 2013; Mei et al. 2015; Li et al. 2015). However, our method accurately captures the eastward-propagating nature of the MJO (see Fig. S2 in the supplemental material for an example). For some events that are not initiated over the western Indian Ocean as classical MJOs, we noticed that before the organized eastward propagation, there might be weak but stationary convective activities on the intraseasonal time scale, which should not be considered as a stage of MJO and are excluded with our method.

b. *Cluster analysis result of MJO initiation regions*

With the MJO events and their initiation longitudes identified, the cluster analysis method (Kaufman and Rousseeuw 2005; Everitt et al. 2011; Wierzchon and Klopotek 2018) is adopted to objectively group the MJO initiation regions into a few longitude zones. To obtain an optimum result, the hierarchical clustering and the *k*-means clustering methods with a variety of parameter settings (including the number of clusters, distance metrics and linkage methods) are tested, for samples of total events (including wet and dry) and for wet and dry events only.

After comparison, we find that the "Euclidean" distance metric and the "average" linkage method are the most straightforward for clustering spatial distance variables such as the initiation longitudes. The dendrogram of the hierarchical cluster tree (Fig. S3a in the supplemental material) suggests that setting the number of clusters to two or four would be optimum. However, it is too rough to depict the diversity of MJO initiation regions with only two longitude zones. Therefore, we decided to group the initiation regions into four longitude zones with the help of the hierarchical clustering. The mean silhouette value of which (Fig. S3b in the supplemental material) is also among the highest in all tested clustering results. A very similar result is given by the *k*-means clustering method when the number of clusters is set to four. Almost the same results are obtained for total events and for wet or dry events only. There are a few cases with negative silhouette values at the edges of each cluster. Those events are excluded to eliminate uncertainties, which also makes the longitude zones more distinguishable from each other.

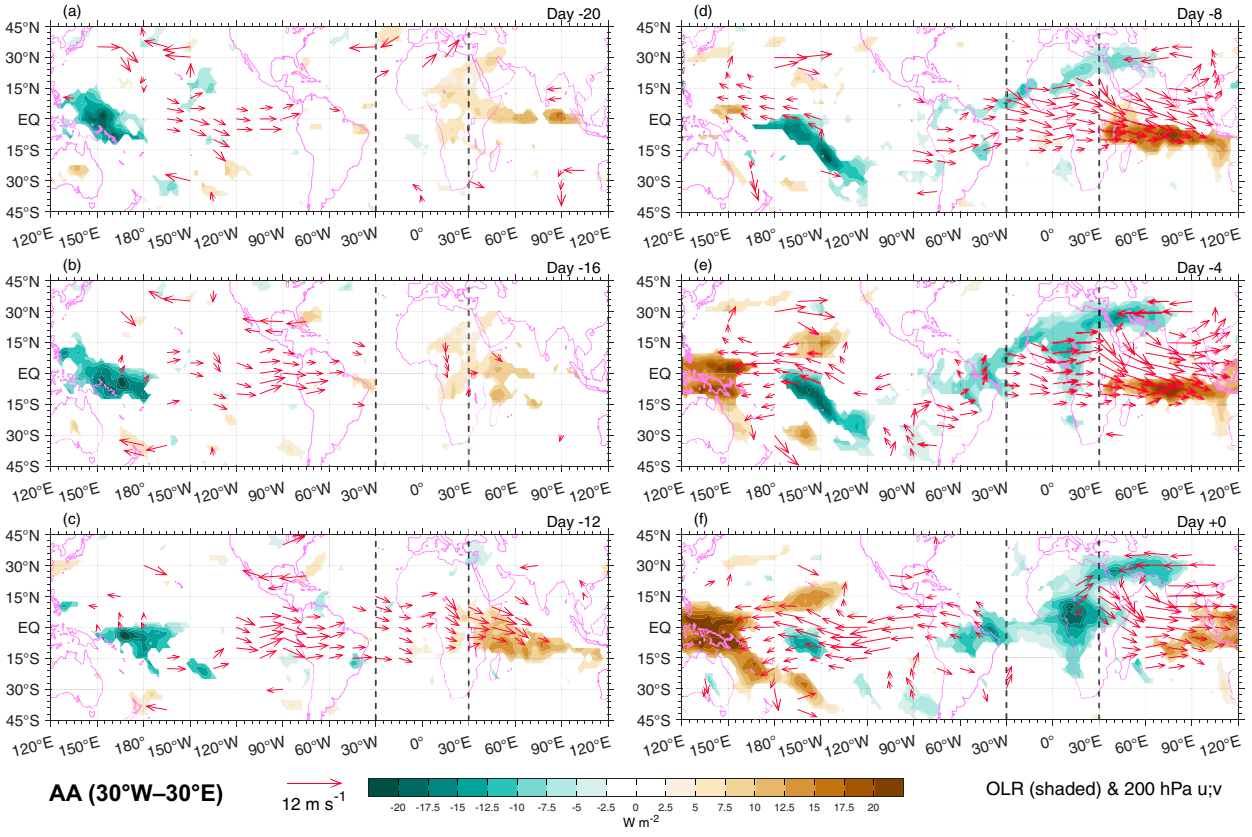

FIG. 4. Longitude–latitude diagrams of composite intraseasonal anomalies of OLR (shaded) and 200-hPa horizontal winds (vectors) for the MJO wet events initiated over the AA region.

The final result of the cluster analysis for MJO initiation regions is shown in Fig. 1. According to their geographical locations, the four longitude zones are referred to as (from west to east): Atlantic and Africa (AA; 30°W–30°E), Indian Ocean (IO; 40°–85°E), Maritime Continent (MC; 95°–130°E), and western Pacific (WP; 135°E–180°). There are 18, 71, 12, and 7 wet events identified in each region, respectively. As expected, the Indian Ocean and the Atlantic and Africa are most favorable for MJO initiations (Wang and Rui 1990), whereas some uncertainties might exist for the WP group since only a few events were identified there. Although the east Pacific warm pool is a well-documented region of intraseasonal convective variability during boreal summer (Maloney and Esbensen 2003), no event was detected in this region according to our criteria since we focus on the winter season. Figure 1 also shows that the distributions of total (wet plus dry) events and wet events are similar.

4. Precursory signals and processes associated with MJO initiation over each region

In this section, the precursory signals and processes associated with the MJO initiation over each longitude zones will be studied. Only the initiations of wet events (MJO convectively active phase) are concerned. The lead–lag composite analyses are conducted for the intraseasonal (20–80-day temporal filtered) anomalies. The initiation date is referred to as day 0, and positive (negative) days indicate the time after (before) it. The spatial variables associated with each event are slightly shifted in zonal direction before the composite, so as to align the initiation longitude at the center of the longitude zone. In another word, the composite is conducted as if all the events are initiated at a same longitude. This amplifies the precursory signals containing the information of relative position, though at the cost of losing representativeness of longitude and topography.

The statistical significance of composite anomalies is assessed by a two-sided nonparametric rank-sum test, with a null hypothesis that the composites have equal means of the climatology. Following Wilks (2006, 2016), the false discovery rate (FDR) (Benjamini and Hochberg 1995) is controlled at the level $\alpha_{\mathrm{FDR}} = 0.15$. The local null hypotheses are rejected if the respective p values are smaller than the threshold value p^*_{FDR} [see Wilks (2006, 2016) for details]. A relatively higher α_{FDR} is chosen because there are not enough cases (less than 30) in the regions other than the IO. A too strict α_{FDR} (say, 0.05) results in unorganized composite diagrams. We have to strike a balance between the statistical significance and the physical interpretation. According to Wilks (2016), for moderate and strong spatial

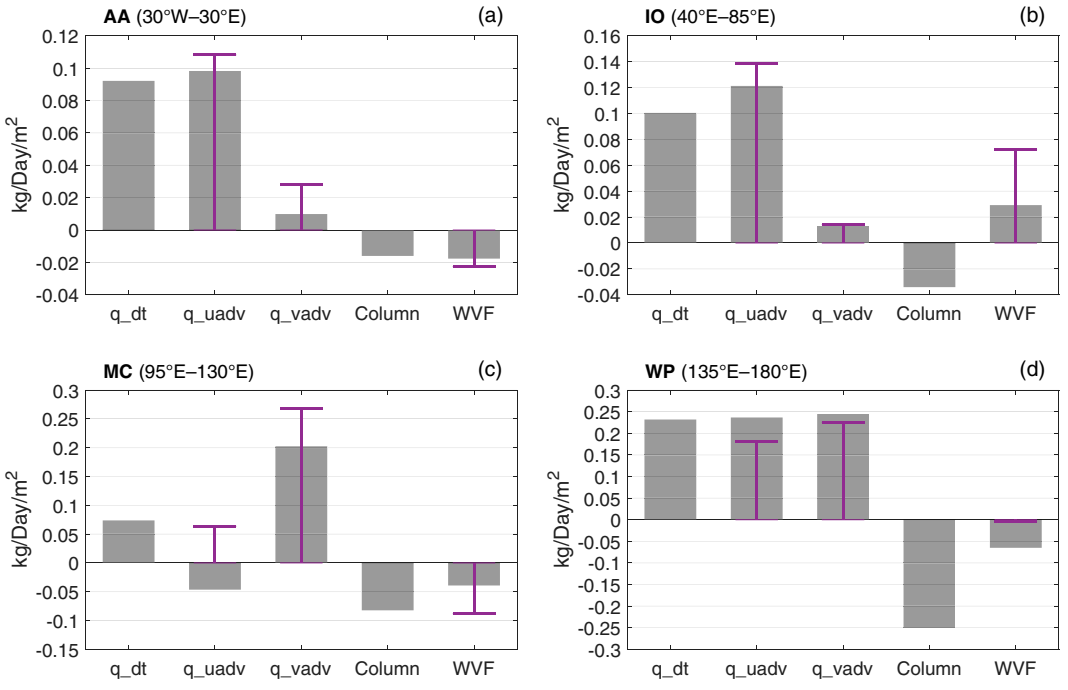

FIG. 5. The 1000–500-hPa moisture budget diagnosis results from lead/lag days −12 to −3, averaged over 15°S–10°N and longitude zones of (a) AA, (b) IO, (c) MC, and (d) WP. The gray bars indicate (from left to right) the composite intraseasonal anomalies of local tendency, zonal advection, meridional advection, column process, and surface upward water vapor flux. The purple "T" mark over the corresponding bars indicates the advection of low-frequency background moisture by the intraseasonal flow ($-\langle \mathbf{V}'\nabla\overline{q}\rangle'$, where $\mathbf{V}$ is the horizontal wind), or the water vapor flux contributed by the intraseasonal sea–air specific humidity differences $[\overline{(\rho c_e)}\,\overline{U}\Delta q']$.

correlation (which is typically the case for intraseasonal filtered variables), it is approximately that the global test level $\alpha_{\text{global}} = (1/2)\alpha_{\text{FDR}} = 0.075$.

a. Atlantic and Africa (AA)

Figure 2 shows the longitude–lead/lag time diagrams of the composites of MJO wet events initiated over the AA region, with the initiation longitudes aligned. The significant MJO active convection emerges after day −5 (denoted by the gray line) and propagates eastward, whereas hardly any convective anomalies can be detected inside the longitude zone before the initiation (Fig. 2a). On the other hand, there is a clear eastward propagating upper-tropospheric westerly anomaly (Fig. 2b, shading). The vertical and horizontal cross sections indicate that the westerly anomaly originates from the upper-tropospheric Kelvin wave response of the active intraseasonal convection over the western Pacific (Figs. 3 and 4, from days −20 to −16). The latter also shows a slowly eastward-propagating feature that can be traced back to the eastern Indian Ocean (Fig. 2a), and could be a previous active phase of MJO.

The active convection over the western Pacific propagates eastward and decays rapidly near the date line (Figs. 3 and 4, from days −12 to −4). As a result, the upper-tropospheric westerly anomaly decouples from the convection and keeps propagating eastward at a much faster speed close to that of a free atmospheric Kelvin wave (5.9 m s^{-1} before and 32.2 m s^{-1} after decoupling; see the red lines in Fig. 2b), acting like a circumnavigating signal (Knutson et al. 1986; Milliff and Madden 1996; Sobel and Kim 2012). The descending branch ahead (to the east) of the upper-tropospheric westerlies is very weak, but is significantly enhanced as it arrives at the western Indian Ocean.

It is speculated that the enhancement of the subsidence anomaly over the western Indian Ocean (30°–90°E after day −16) is achieved mainly through a positive circulation–convection–moisture feedback. Namely, an external subsidence forcing inhibits the background convection and causes a negative diabatic heating anomaly there. The increased boundary layer divergence as a response to the negative diabatic heating anomaly suppresses upward moisture transport, which further weakens the convection and amplifies the subsidence anomaly [see a schematic diagram in Wang and Li (2021)]. The negative diabatic heating anomaly is key in this positive feedback process, and the active background convections over the moist and warm Indian Ocean precondition it. The external subsidence forcing here is mainly contributed by the upstream circumnavigating upper-tropospheric westerlies, but is not from the downstream vertically overturning circulation of the preceding active MJO convection over the western Pacific. Actually, there is hardly any significant subsidence anomaly over the western Indian Ocean at around day −20, implying a weak downstream forcing. As this preceding active MJO convection moves eastward and decays (from days −20 to −8, 120°E–150°W), its downstream forcing should be even

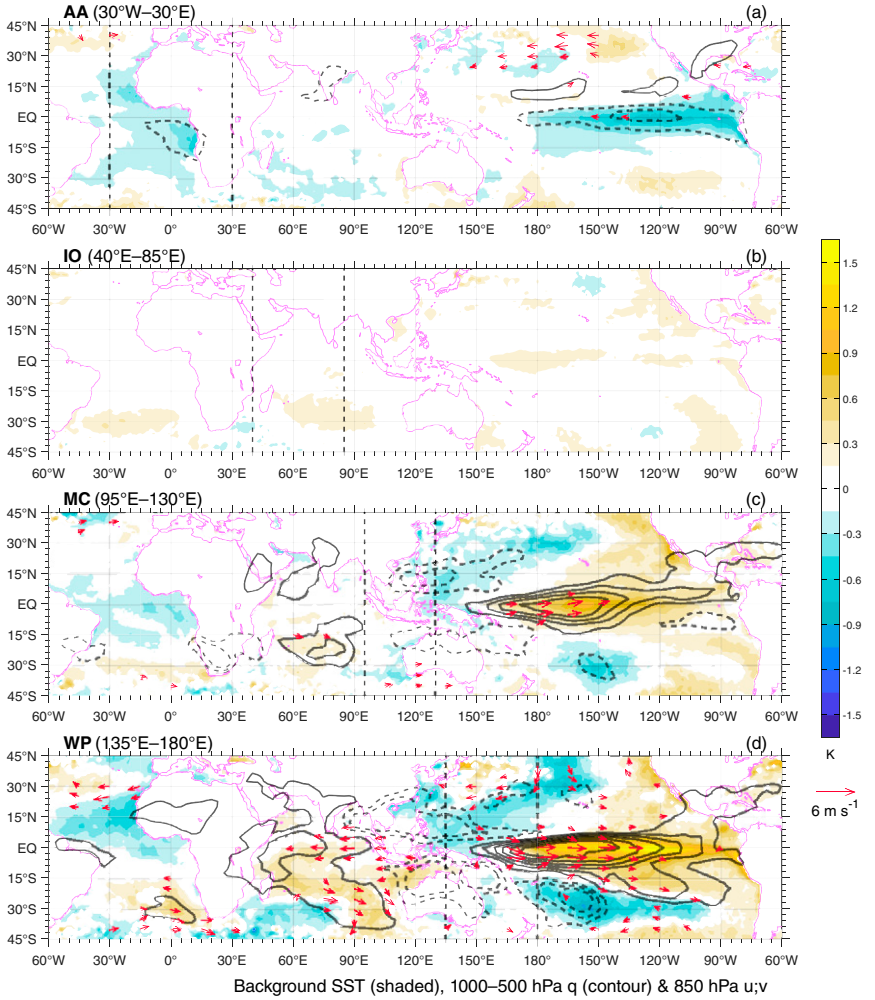

FIG. 6. Composite background (80-day low-pass filtered) anomalies of SST (shaded), 1000–500-hPa averaged specific humidity (contours; 0.2 g kg^{-1} interval with zero omitted, solid for positive and dashed for negative values), and 850-hPa horizontal winds (vectors), from lead/lag days −20 to +10 for the MJO wet events initiated over the (from top to bottom) AA, IO, MC, and WP regions, respectively. Only statistically significant signals based on the FDR approach with $\alpha_{FDR} = 0.15$ are shown.

weaker, contradicting the enhancement of the subsidence anomaly over the western Indian Ocean (30°–90°E).

The enhanced descending causes a low-level easterly anomaly through ER wave response that transports higher background moisture over the Indian Ocean to the west (Fig. 3, right panel). A low-level moisture budget diagnosis shows that such a zonal advection process is the primary contributor of the moistening over the AA before the MJO initiation (Fig. 5a). The zonal moisture advection from east of the initiation region is similar to the downstream process in Zhao et al. (2013) for western Indian Ocean initiation. However, here, in the AA, the descent perturbation of the upstream circumnavigating signal plays a crucial role in causing the low-level easterly anomaly, which is absent in the downstream forcing scenario proposed by Zhao et al. (2013).

The ascending branch to the west of the upper-tropospheric westerlies appears to have triggered an active convection over the Amazon region (60°–30°W) after day −10, possibly supported by topographic lifting. Although it is disconnected from the eastward propagation of the MJO initiated over the AA region (Fig. 2a), it might be helpful in supporting the low-level easterly anomaly through a vertically overturning circulation during the MJO initiation over the AA (Fig. 3, right panel).

In contrast to the upper level, there is no significant and continuously eastward-propagating low-level easterly anomaly before the AA initiation (Fig. 2b, contours). In this case, the role of convergence of circumnavigating low-level Kelvin wave easterly (e.g., Kikuchi and Takayabu 2003; Chen and Zhang 2019) should be minor.

In the above scenario, the upstream circumnavigating signal triggers MJO initiation over the AA. However, its direct

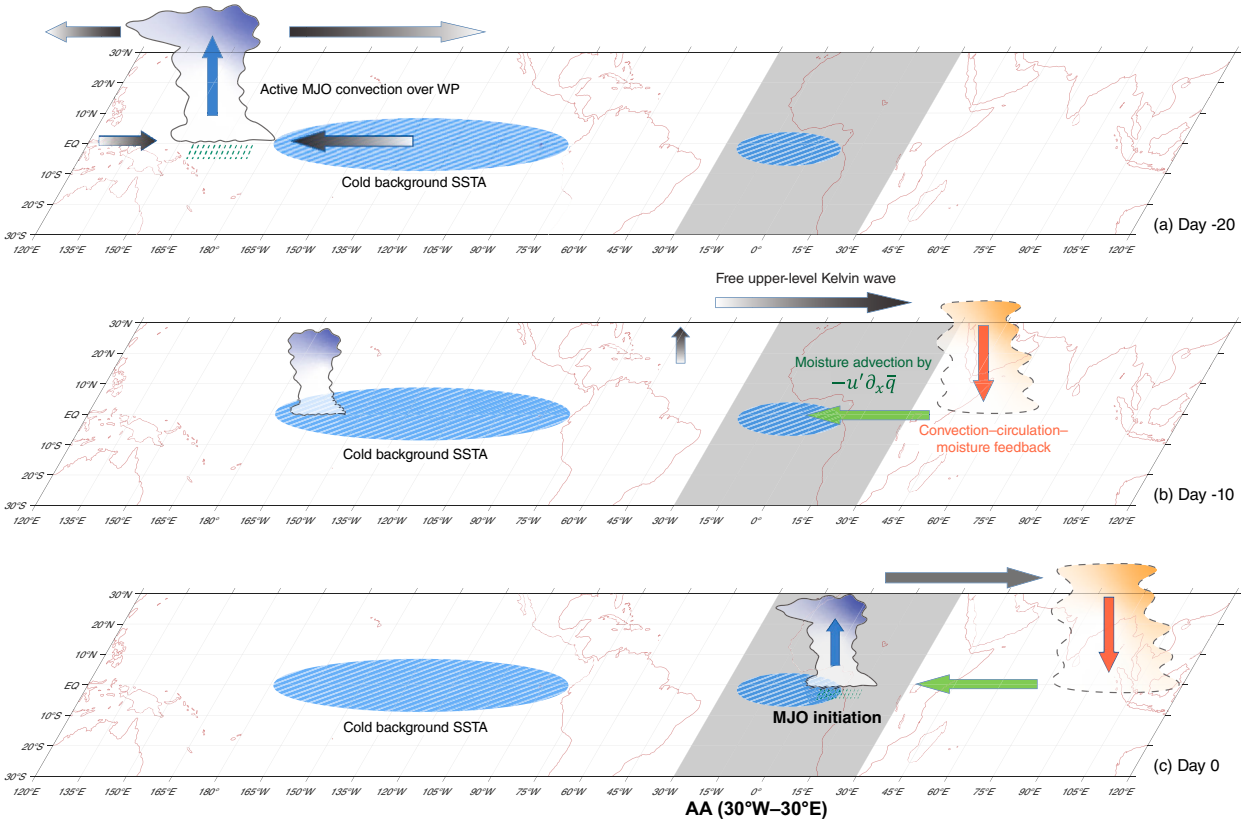

FIG. 7. A schematic diagram of MJO convection initiation over the AA region. Gray areas in the map denote the longitude zone of the initiation region. The blue shading with white stripes denotes the cold background SST anomaly. A cloud with solid edge and blue shading represents an active intraseasonal convection (or its decaying stage if without an anvil in the top and precipitation in the bottom). A cloud with dashed edge and orange shading represents an intraseasonal convectively suppressed anomaly. Straight thick arrows indicate intraseasonal zonal or vertical circulations. Particularly, horizontal green arrows indicate positive advections of background moisture by the low-level intraseasonal flows. A downward orange arrow implies a positive convection–circulation–moisture feedback that amplifies the anomalous subsidence.

forcing, including the low-level convergence and the ascending branch, plays a secondary role. Rather, the descending branch ahead of the upper-tropospheric Kelvin wave westerlies plays a crucial role, through a relay effect of the warm and moist Indian Ocean.

The low-frequency background anomalies (80-day low-pass filtered) associated with AA initiation are explored (Fig. 6a). A La Niña–like background SST pattern is found to be favorable of AA initiation. On one hand, the warm western Pacific (although not significant as controlled by the FDR) maintains a strong MJO convection there. On the other hand, the cold eastern Pacific makes the MJO convection decays rapidly after it moves out of the warm pool, so that the upper-tropospheric westerlies are more readily to decouple from the convection. In addition, significant cold and dry background anomalies are found extending from the date line all the way to the west coast of Africa, while the Indian Ocean is close to the normal. The circulation–convection–moisture feedback is thus inhibited over the cold oceans, so that the descent branch should not be enhanced until it arrives at the western Indian Ocean.

Figure 7 is a schematic diagram illustrating the precursory signals and processes associated with the AA initiation. For the sake of brevity, detailed explanations of the schematics will be provided in section 5.

b. *Indian Ocean*

The longitude–lead/lag time diagrams of composite intraseasonal anomalies associated with the MJO initiation over the Indian Ocean (IO) region are shown in Fig. 8. The composite MJO behaves as continuous and alternating occurrences of wet and dry events over the IO propagate eastward, just like the classical MJO. In comparison to the AA initiation, hardly any statistically significant and continuously propagating upstream signals associated with the IO initiation can be detected. The preceding MJO wet phase in the IO initiation (Fig. 8a, from days −40 to −10) also propagates for a shorter time period and decays earlier than that in the AA initiation (Fig. 2a, from days −40 to 0), as the latter successfully passed through the date line and propagated another 30° in longitude, while the former failed. Given the fact that IO locates to the east of AA, it would be much more difficult for

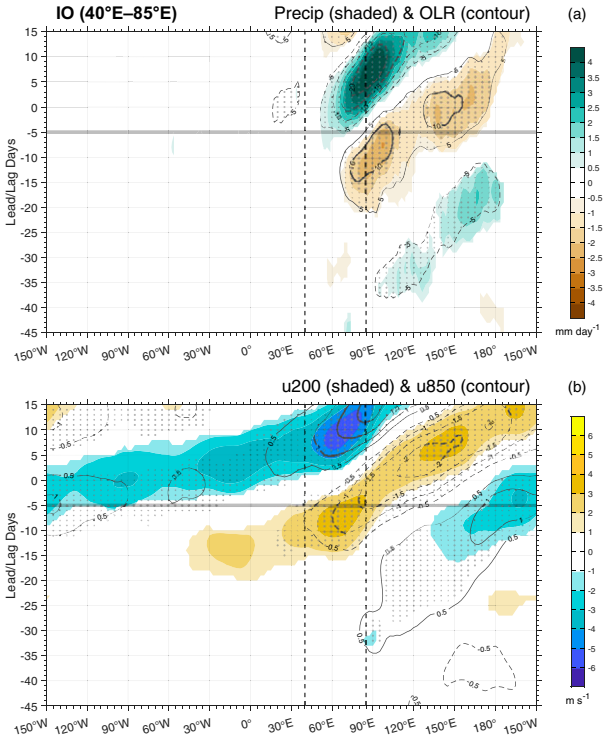

FIG. 8. As in Fig. 2, but for MJOs initiated over the IO region.

the preceding MJO wet phase to exert an upstream effect to the IO longitude zone, simply because of the longer distance.

The above facts imply that rather than the upstream forcing, the downstream effect by the preceding MJO dry phase could be more important to the MJO wet phase initiation over the IO, as reported in previous studies (Zhao et al. 2013; Li et al. 2015). The vertical cross section (Fig. 9) shows that for a wet (dry) MJO initiated over the IO region, the eastward zonal distance to the preceding dry (wet) event is short, not longer than 90° in longitude. In an idealized scenario, the descending branch of an equatorial deep convective heating is located approximately 90° west (or 270° east) of the convection, since the equatorial Kelvin wave has about 3 times the speed of the equatorial Rossby wave (Matsuno 1966; Gill 1980). This implies that 90° in longitude is a potential upper limit of downstream forcing distance of the ER wave response to deep convective heating. The vertically overturning circulations within a zonal scale of 90° between those successive wet and dry events are clearly identified in Fig. 9 for the IO scenario, indicating a strong downstream forcing via ER wave response. In contrast, such a downstream effect is not as evident at the early stage of the AA initiation.

As the preceding MJO dry phase propagates eastward, the associated low-level easterly anomaly transports higher background moisture to the western Indian Ocean (Fig. 9, from days −12 to 0). This is the dominant factor in the moistening over the IO during the preinitiation stage, as confirmed by the moisture budget diagnosis (Fig. 5b). Such a downstream forcing procedure agrees with previous studies (Zhao et al. 2013; Mei et al. 2015; Li et al. 2015).

In addition to the moisture advection, the surface upward water vapor flux also contributes positively in the IO initiation, which is the only case among the four regions (Fig. 5). The positive WVF anomaly over the IO is dominantly contributed by the increased sea–air specific humidity difference [Eq. (4)]. As shown in Fig. 10, a warm SST anomaly emerges over the IO as the preceding MJO dry phase develops and propagates eastward. This significant warm SST anomaly is jointly caused by the reduced near-surface wind speed (easterly anomaly of the dry phase against the mean surface westerly in winter), the increased insolation due to suppressed convection, and the shallower mixed layer in winter (Waliser et al. 2003, 2004; Li et al. 2008). As a result, this warm SST anomaly exerts a delayed effect to the upcoming MJO wet phase through increasing the WVF and low-level instability, implying a two-way air–sea interaction scenario on the intraseasonal time scale (Li et al. 2008).

Since the IO initiation is the most frequent, there is no organized and significant background anomalies associated with it (Fig. 6b). Figure 11 is a schematic diagram summarizing all relevant initiation processes in IO.

c. *Maritime Continent*

Several features are noticed in the longitude–lead/lag time diagram of composite intraseasonal OLR and precipitation anomalies associated with the MJO initiation over the Maritime Continent (MC) region (Fig. 12a, Fig. S4a in the supplemental material). First, to the west of the MC longitude zone there is hardly any statistically significant signal prior to the large-scale eastward propagating convection. This indicates that the MC initiation events identified here are relatively independent, and should not be considered as a stage of the "jumping" type of the MJO (Wang et al. 2019). The "jumping" type has a preceding eastward propagation over the Indian Ocean, which is disrupted by the Maritime Continent barrier (Zhang and Ling 2017) while another convective region emerges over the western Pacific. Second, before the organized eastward propagation, there exist weak and quasi-standing convective activities inside the MC longitude zone. They last about 10 days and therefore could be regarded as an intraseasonal disturbance, but not the MJO since they are stationary. Finally, a westward-propagating suppressed convection anomaly from the east is detected before the MJO initiation.

The westward-propagating suppressed convection anomaly from the east is the most prominent precursory signal. By examining the associated low-level horizontal circulations (Fig. 13, left panel) and its propagating speed (about 3.9 m s^{-1}), we speculate that it is a dry phase of convectively coupled ER wave (Wang 1988; Wang and Xie 1996; Xie and Wang 1996). The low-level anticyclonic gyres on both sides of the equator are clearly identified. The geographical location and propagation of the circulation anomalies are coherent with the suppressed convection anomaly (Figs. 12 and 13), considering that the ER wave circulation response shifts westward (Matsuno 1966; Gill 1980). Due to extratropical disturbances in the Northern Hemisphere, the symmetry of the anticyclonic gyres about the equator is not

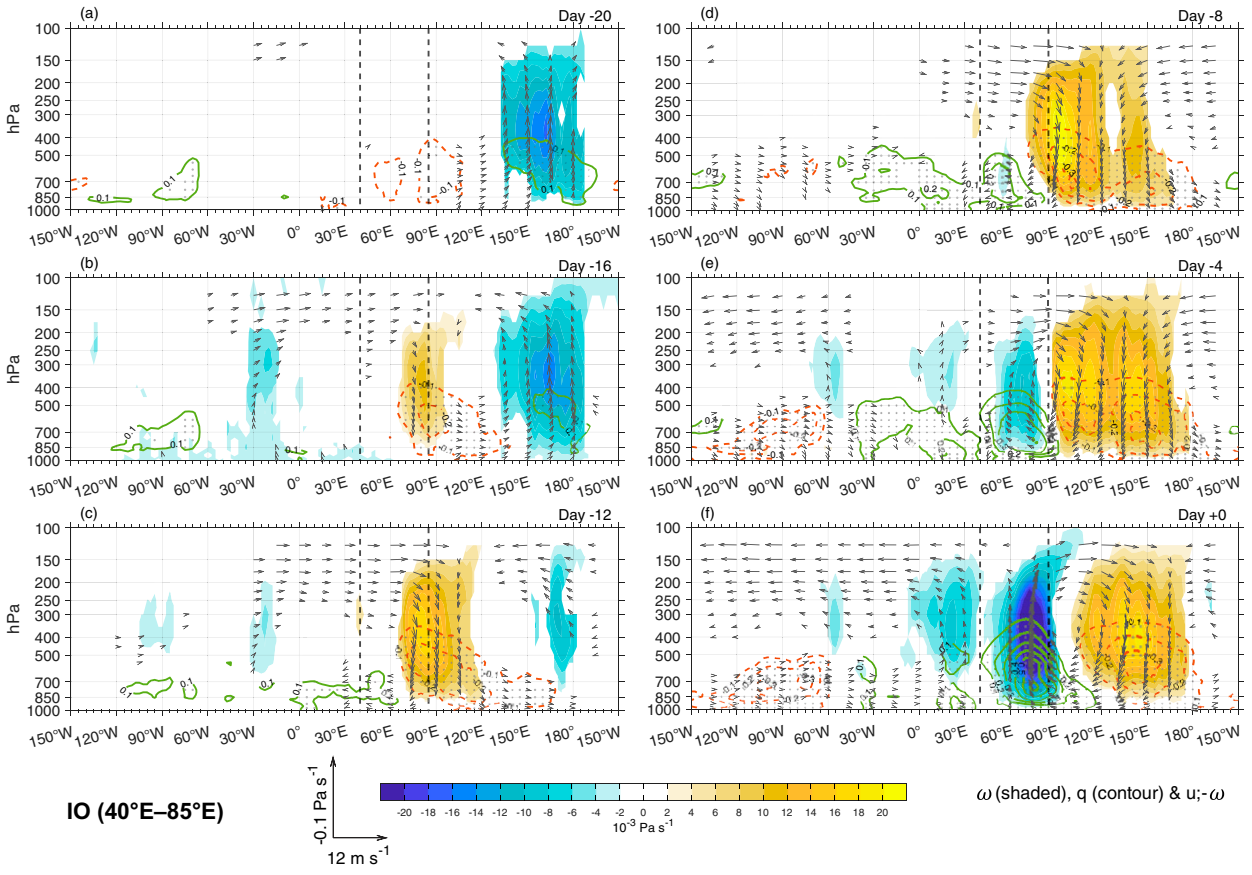

FIG. 9. As in Fig. 3, but for MJOs initiated over the IO region.

quite clear before day −12. The Southern Hemisphere cell is more prominent possibly because it is propagating within a more favorable background (i.e., the South Pacific convergence zone). In this case, only the Southern Hemisphere components are shown for the convection and low-level relative vorticity anomalies in the longitude–lead/lag time diagrams (Fig. 12). As this suppressed convection anomaly moves westward, it is enhanced through a same positive feedback mechanism between circulation and negative diabatic heating anomaly described before. The associated ER wave response also begins to dominate the equatorial circulation anomaly and makes it more symmetric about the equator (Fig. 13, day −6 in left panel).

The background state associated with MC initiation shows a weak El Niño–like SST pattern (Fig. 6c). This weakens the background zonal moisture gradient between the warm pool and eastern Pacific, but sharpens the meridional gradient around the MC region. In addition, the warm and moist background near the date line preconditions a positive circulation–convection–moisture feedback, favoring the enhancement of a westward-propagating dry ER wave.

The low-level circulation associated with the dry ER wave contributes moisture advections to the west (Fig. 5c). With the background moisture pattern described above, unlike those in the AA and IO initiations, the zonal advection becomes less important. Instead, the poleward flows of the twin anticyclonic ER wave gyres play an important role, as the mean moisture is maximized along the equator, and such a meridional gradient is sharpened by the El Niño–like background SST pattern.

This meridional moisture advection procedure is similar to one of the MJO propagating mechanisms in the view of moisture mode theory (Kim et al. 2014; Wang et al. 2017). In the theory proposed by Kim et al. (2014), the descending branch in front of the MJO convection causes a negative diabatic heating anomaly and anticyclonic low-level ER wave response. The strength of the descent finally determines whether the MJO propagates or not. Here for the MJO initiation over the MC, the poleward flows arise from a dry ER wave intrusion.

What causes the quasi-standing convection anomaly over the MC before the large-scale eastward propagation takes place, and why it becomes an eastward-propagating MJO afterward? It is possible that this quasi-standing convection anomaly arises from cooperative interactions between eastward and westward convectively coupled intraseasonal perturbations (Zhang and Hendon 1997; Roundy and Frank 2004), and the precursory dry ER wave may play a role in it. The evolution of the low-level moisture anomaly (contours in the right panel of Fig. 13) suggests that before day −5, large-scale dry anomalies associated with the ER wave locate east of the

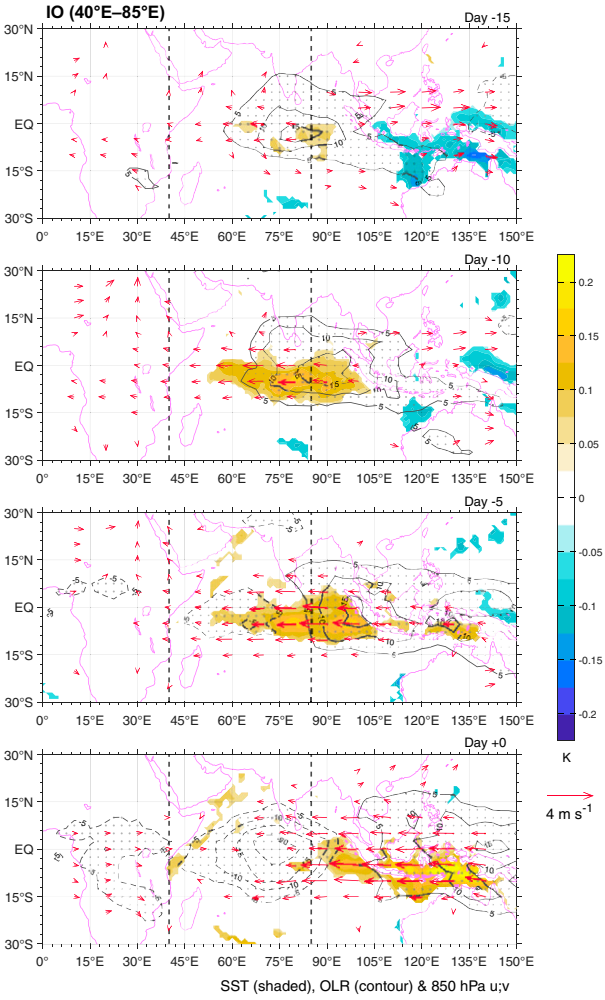

FIG. 10. Composite intraseasonal anomalies of sea surface temperature (shaded), OLR (contours; 5 W m^{-2} interval with zero omitted), and 850-hPa horizontal winds (vectors) for the MJO wet events initiated over the IO region.

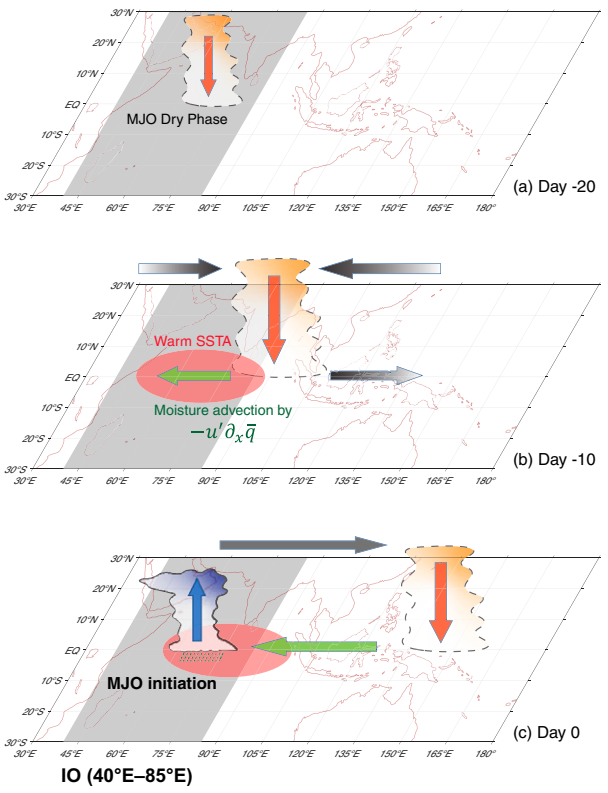

FIG. 11. A schematic diagram of MJO convection initiation over the IO region. The red shading denotes the intraseasonal warm SST anomaly. Other implications of the elements are same as in Fig. 7.

MC region. This inhibits the eastward propagation of the convective activities over the MC. On the other hand, the poleward flows of the ER wave gyre moisten the MC region through advecting background moisture, promoting the convection developing in situ. Once deep convection is triggered, the intruding ER wave from the east is gradually replaced by a strong Kelvin wave response (Fig. 13, day 0). The boundary layer convergence of the Kelvin wave causes an asymmetric zonal moisture distribution that tilts eastward and downward. Such a boundary layer moisture leading structure is one of key factors determining the MJO eastward propagation (Hsu and Li 2012).

Some past studies suggest that dry ER wave precursors propagated from east of the MC sector stifle the MJO propagation (Feng et al. 2015; Demott et al. 2018), which seems a bit at odds with the MC initiation mechanism proposed here. However, we argue there are two major differences. First, what we are studying is the mechanism of initial onset of MJO convection before it moves eastward, while those past studies care about how an MJO passes through the MC barrier. The latter is essentially a propagating mechanism. Second and the most important, the MC initiations are associated with a specific background state (El Niño–like SST pattern), which makes the moisture advections different from those proposed in the past studies. A dry ER wave stifles the MJO propagation mainly through advecting dry subtropical air into the tropics (Demott et al. 2018) and dry eastern Pacific air westward (Feng et al. 2015; Demott et al. 2018). The mean easterly also advects anomalous dry air of the ER wave westward (Feng et al. 2015). The above scenario is more frequent during La Niña (Demott et al. 2018). In contrast, during El Niño, the eastern Pacific is moister and the mean easterly is weakened (Fig. 6c). Meanwhile, the poleward flows of the ER wave cooperate with a sharpened meridional moisture gradient over the MC, resulting in a positive moisture advection and promoting the convection initiation there. The dry ER wave is thus replaced by a Kelvin wave response associated with abundant low-level moisture. This also gives a hint that during El Niño, it is possible that a dry ER wave from the east promotes the MJO eastward propagation rather than hinders it.

Figure 14 illustrates all essential processes of MJO initiation over MC.

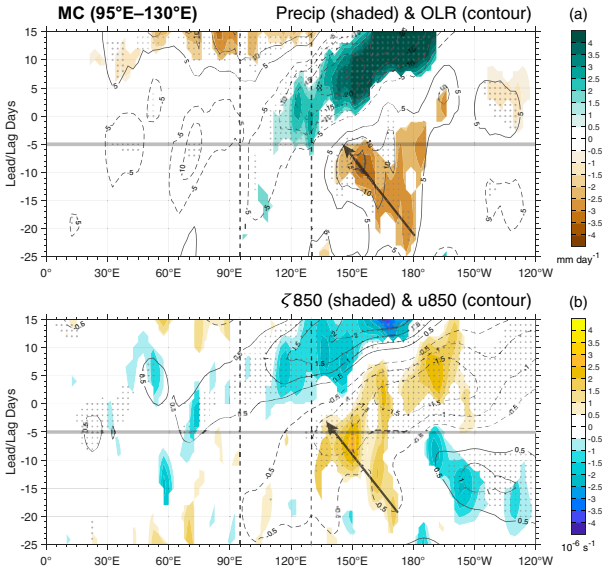

FIG. 12. Longitude–lead/lag time diagrams of composite intraseasonal anomalies of (a) precipitation (shaded) and OLR (contours; 5 W m^{-2} interval with zero omitted) averaged over 0°–15°S; and (b) 850-hPa vorticity averaged over 5°–20°S (shaded) and 850-hPa zonal wind averaged over 15°S–10°N (contours; 0.5 m s^{-1} interval with zero omitted), for the MJO wet events initiated over the MC region. A thick arrow indicates a westward-propagating signal with a mean speed of 3.9 m s^{-1}. Some variables are averaged south of the equator because their corresponding precursory signals are more confined to the south. The lead/lag time is cut off at day 225 to highlight the precursory signals of the dry ER wave. Figure S4 in the supplemental material gives the diagrams for MC initiation with the same settings used in the other regions.

d. Western Pacific

There are only a few wet event initiations identified over the western Pacific (WP) region (7 in total). The composite longitude–lead/lag time diagrams (Fig. 15) seem a little bit noisy. Those standing, westward and eastward-propagating signals are evident, implying complicated interactions of convectively coupled intraseasonal perturbations (Zhang and Hendon 1997; Roundy and Frank 2004). The convective activities inside the WP longitude zone show an oscillating feature of short period that approaches the quasi-biweekly time scale. Two branches of eastward-propagating low-level zonal wind anomalies (Fig. 15b, contours) are found disrupted over the MC region but reemerge to the east, suggesting the corresponding convective anomalies might resemble the "jumping" type MJO suggested by Wang et al. (2019).

The most prominent precursory signal of the WP initiation is a suppressed convection anomaly that originates inside the WP longitude zone and propagates eastward. A further examination of the horizontal maps and vertical cross sections (Fig. 16) reveals its equatorial-trapped and slowly eastward-propagating (about 2.9 m s^{-1}) features, all agree with the characteristics of the MJO. Therefore, we argue that the initiation of the MJO wet phase over the WP has a similar downstream forcing scenario as in the IO. That is, a preceding MJO dry phase that propagates eastward brings moisture advection through the low-level ER wave response.

The associated background state of the WP initiation (Fig. 6d) supports the downstream forcing scenario. Similar to those in the MC initiation, an El Niño–like background SST pattern is found, accompanied with increased moisture and weakened mean easterly over the central and eastern Pacific, and a sharpened meridional moisture gradient inside the WP longitude zone. In comparison to the MC initiation (Fig. 6c), the background warm SST over the eastern Pacific is much stronger and shift eastward in the WP initiation. The corresponding eastern Pacific moisture also has a much higher departure from the climatology, favoring MJO activities near and east of the date line.

In the existence of above background state, a low-level moisture budget analysis (Fig. 5d) suggests that the westward and poleward low-level anomalous flows of the preceding suppressed phase of MJO advect background moisture to the WP region. The two processes have almost equivalent strength. The anomalous low-level moistening first takes place in the MC sector and moves eastward as the suppressed phase of MJO moves (Fig. 16, right panel). However, the convection was not developed to the west of the WP longitude zone where background is relatively colder and drier during El Niño. The initiation takes place until the anomalous moistening encounters the higher background moisture inside the WP longitude zone.

Figure 17 provides a schematic diagram for MJO initiation in WP.

5. Summary and discussion

a. Summary

We explored the diversity of MJO in terms of its initiation, which refers to the initial onset of active convection before it moves eastward. First, the MJO events are identified around the global tropics for boreal winters from 1979/80 to 2018/19, and then an objective clustering method is applied to the initiation longitudes of identified events, so as to group the MJO initiation regions into a few equatorial longitude zones, the Atlantic and Africa sector (AA; 30°W–30°E), Indian Ocean (IO; 40°–85°E), Maritime Continent (MC; 95°–130°E), and western Pacific (WP; 135°E–180°). Next, the precursory signals and processes associated with the MJO initiation over each region are examined through a composite analysis. The MJO initiation mechanism is found to be region-dependent, and is summarized below using the schematic diagrams.

The AA initiation mechanism acts like a circumnavigating scenario, whereas the descending perturbation with the help of a relay effect of Indian Ocean holds the key. The precursory signal can be traced back to an intraseasonal convection over the western Pacific (Fig. 7a), which then moves eastward out of the warm pool and decays (Fig. 7b, shrunk blue cloud) over the La Niña–like colder and drier background (blue shading with white stripes). As a result, the Kelvin wave response

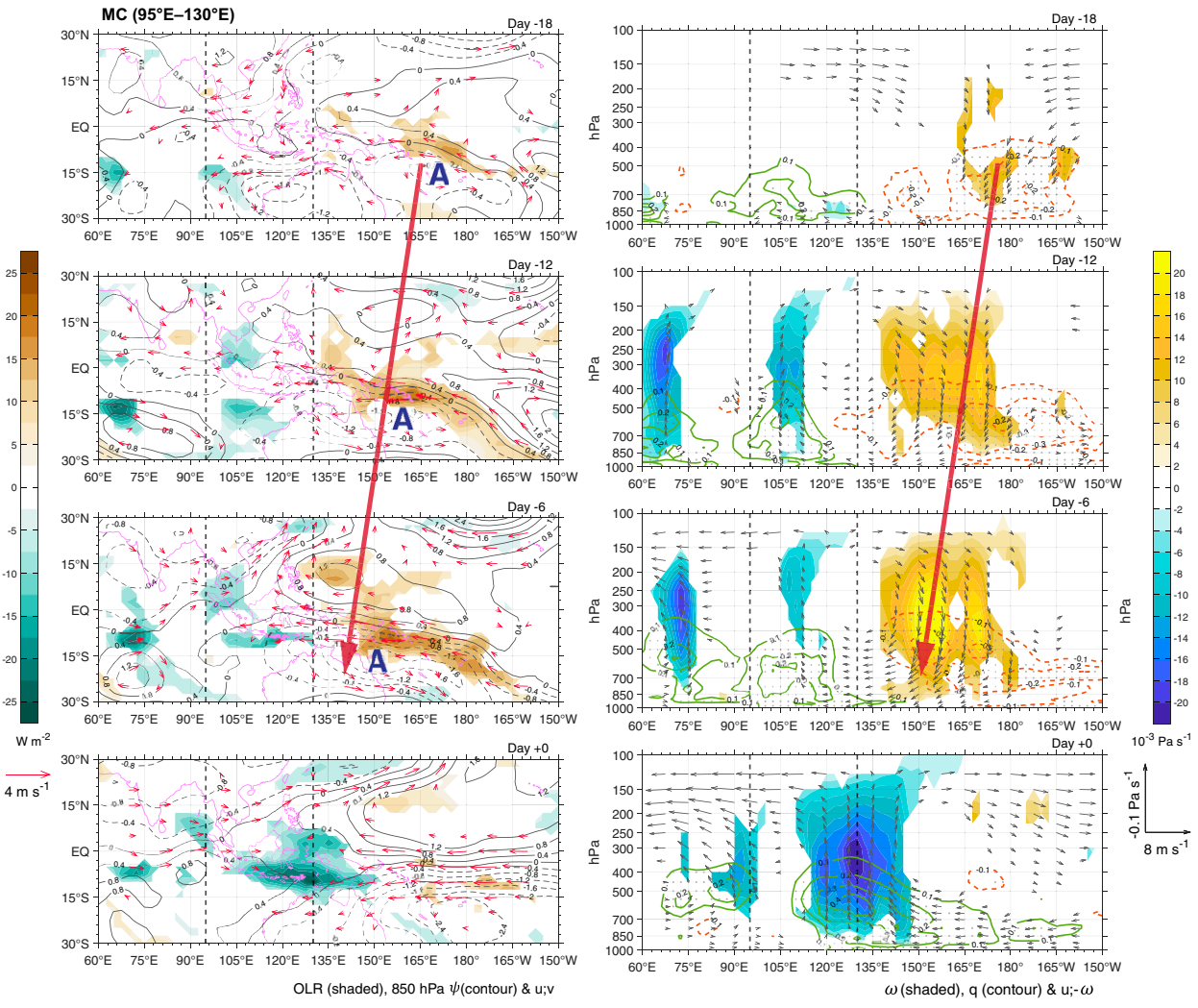

FIG. 13. Composite intraseasonal anomalies for the MJO wet events initiated over the MC region. (left) OLR (shaded), 850-hPa streamfunction (contours; 10^6 m^2 s^{-1}), and horizontal winds (vectors). The streamfunction is calculated based on the composite horizontal winds. (right) As in Fig. 3. The thick arrows have the same implication as those in Fig. 12. The anticyclonic circulation centers associated with the westward-propagating signal are marked by "A" in the left panels.

decouples from the convection, and the upper-tropospheric westerly anomaly propagates eastward at a faster speed (thick black arrow). Once the descending branch ahead (orange arrow) arrives at the western Indian Ocean where convection is climatologically active, it is amplified through a positive feedback with the induced negative diabatic heating anomaly (orange cloud, here indicating that the climatologically active convection is damped). As a result of the ER wave response to the latter, the low-level easterly anomaly transports higher mean moisture west to the AA region (green arrow). This primary process triggers a new MJO convection over the AA (Fig. 7c). Unlike most previous studies that emphasized the direct lifting effect of the circumnavigating disturbance, here we argue that the descending branch of the Kelvin wave holds the key in the convection onset, and the warm and moist Indian Ocean plays a relay role.

The IO initiation arises mainly from the downstream forcing and the delayed air–sea interaction. A preceding convectively suppressed phase of MJO (Fig. 11a) moves eastward and develops (Fig. 11b). The associated low-level easterly anomaly transports mean moisture to the west (green arrow). The intraseasonal warm SST anomaly (red shading) caused by the preceding suppressed phase of MJO generates a delayed effect by increasing the surface evaporation. A successive active MJO convection is thus initiated over the IO (Fig. 11c). The above processes agree with the downstream forcing scenario suggested by Zhao et al. (2013), and the delayed air–sea interaction mechanism proposed by Li et al. (2008).

The MC initiation begins from an ER wave to the east, which propagates westward and is associated with suppressed convection (Fig. 14a, orange cloud). The originally weak and standing intraseasonal convection over the MC (Fig. 14b, blue

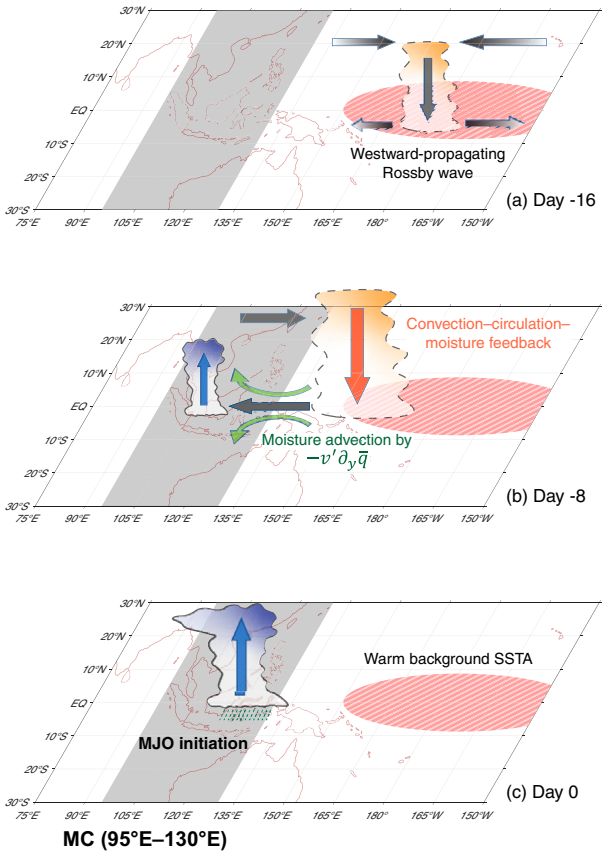

FIG. 14. A schematic diagram of MJO convection initiation over the MC region. The red shading with white stripes denotes the warm background SST anomaly. Other implications of the elements are as in Fig. 7.

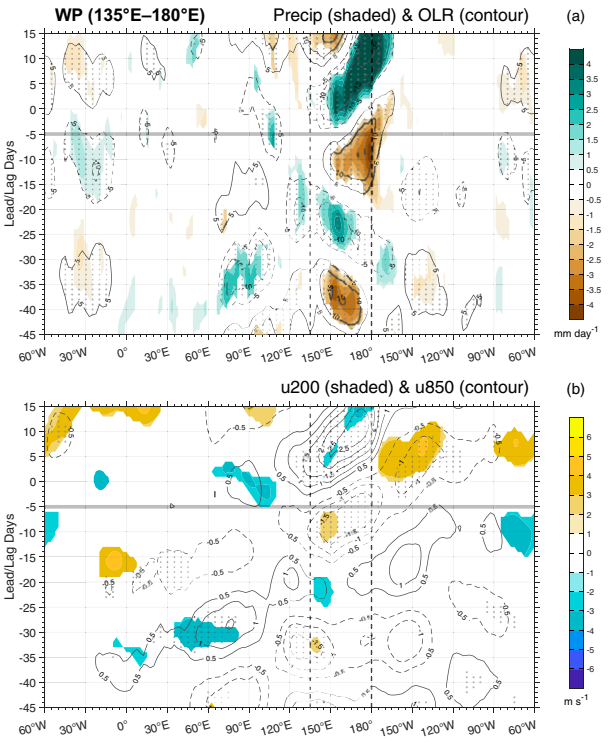

FIG. 15. As in Fig. 2, but for MJOs initiated over the WP region.

cloud) is enhanced by the meridional advection of mean moisture, in which the poleward flows of the twin anticyclonic ER wave gyres play a dominant role (curved green arrows). As long as the intraseasonal convection over the MC intensifies and the dry ER wave decays, the former propagates eastward in the existence of low-level moisture leading, indicating the initiation of MJO over the MC (Fig. 14c). The El Niño–like warm background of the central and eastern Pacific (red shading with white stripes) favors activities of MJOs and convectively coupled ER waves, and also significantly sharpens the meridional gradient of background moisture in the MC sector.

The WP initiation (Fig. 17) is similar to the downstream forcing scenario in the IO. A strong El Niño–like warm background (red shading with white stripes) causes a much higher departure of eastern Pacific moisture from climatology, favoring MJO activities near and east of the date line. It also sharpens the meridional gradient of background moisture inside the WP longitude zone. In this case, both zonal and meridional advections of mean moisture, respectively, by westward and poleward intraseasonal flows of the preceding suppressed phase of MJO are contributing equivalently (Fig. 17b, green arrows). The MJO initiation takes place over the WP when there is abundant moisture (Fig. 17c).

In addition to tropical origins as summarized above, the role of extratropical forcing in MJO initiation has been reported in past studies. We have attempted to explore this possibility in the region-dependent MJO initiation mechanisms. The composite extratropical wave activity fluxes from Northern (Southern) Hemisphere are found convergent to the AA (IO, MC, WP) longitude zone before day 0 (Fig. S5 in the supplemental material), and therefore may play a role in the MJO initiation there. However, details relevant to the extratropical forcing and interactions with the tropical processes require a further case-by-case study.

b. *Discussion*

In comparison to a recent study relevant to the similar issue (Takasuka and Satoh 2021), we identify that AA (Atlantic and Africa) is one of the principal MJO initiation regions, which was reported in previous observational studies (e.g., Wang and Rui 1990) but absent in Takasuka and Satoh (2021). This is because in our study, the MJO events are identified around the global tropics, and the classification of initiation regions is achieved by an objective clustering method. On the contrary, Takasuka and Satoh (2021) subjectively determined the initiation regions in advance. The other three regions are similar, except that the IO in our study shifts westward, which is consistent with the observations (Zhao et al. 2013).

It is worth pointing out that the cluster analysis we applied is an objective method, but "objective" does not imply completely free of human intervention. Similar to other commonly used objective methods (wavelet analysis, for instance),

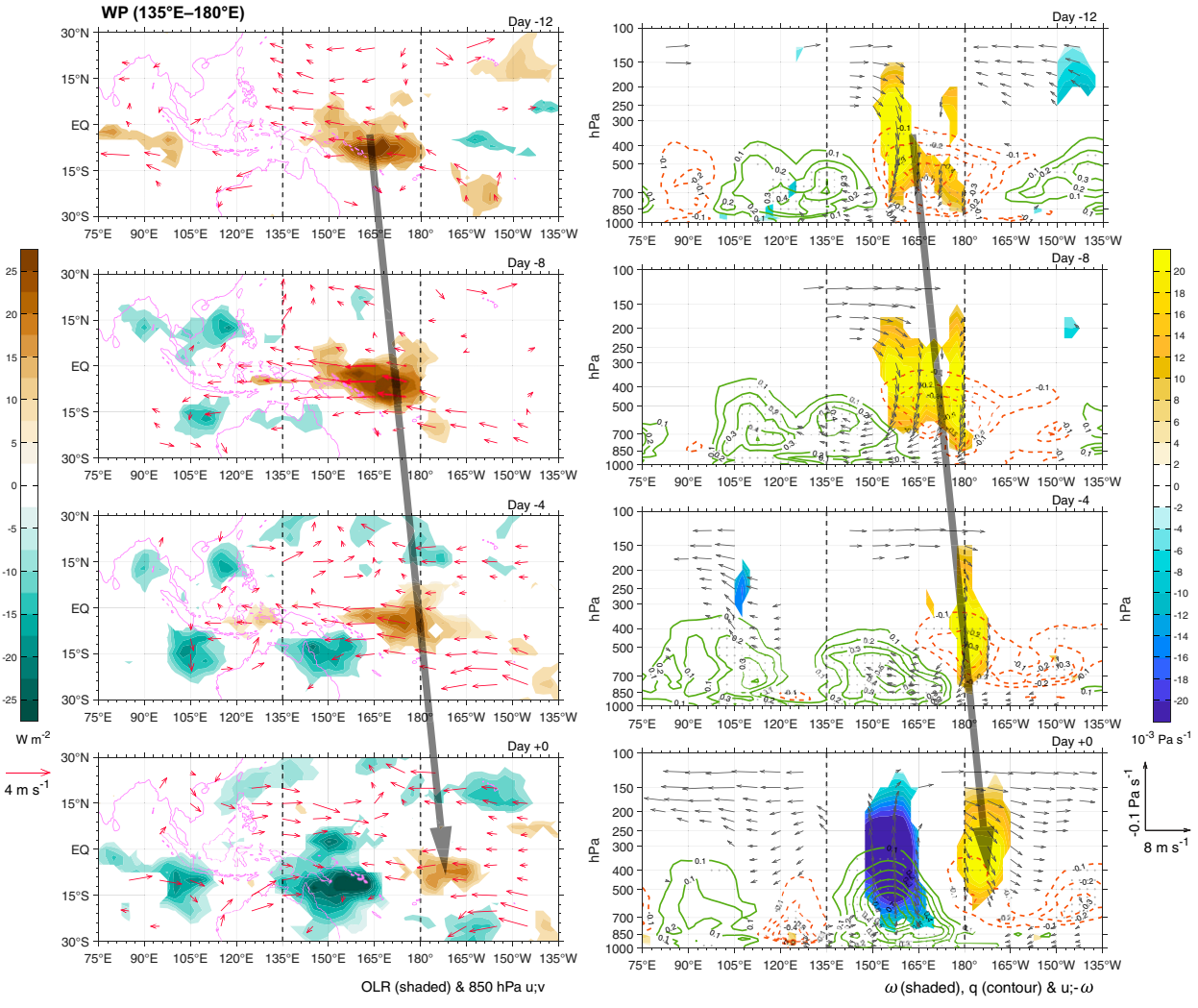

FIG. 16. As in Fig. 13, but for the MJO wet events initiated over the WP region. The thick arrows indicate the eastward propagation of the preceding MJO convectively suppressed phase at a mean speed of 2.9 m s^{-1}.

several tunable parameters need to be set manually in advance. For the cluster analysis, one advantage is that there are objectively obtained supplemental diagrams (such as dendrograms and silhouette values) to help decide which clustering results are optimum. However, uncertainties may still exist, particularly for events at the edges of each cluster. Section 3b describes our clustering procedure.

The initiation mechanism relevant to the diversity of MJO initiation regions is region-dependent. Particularly, we found that the circumnavigating signal that was previously demonstrated not to be crucial in the IO initiation (e.g., Zhao et al. 2013; Ray and Li 2013; Li et al. 2015; Maloney and Wolding 2015) plays a dominant role in the AA initiation. Unlike most previous studies that emphasized the direct lifting effect in the circumnavigating theory, we argue that it is the descending perturbation relayed by a convectively active background that contributes to the new convection onset. For the MC initiation, the ER wave intrusion scenario proposed in our study has also been reported in Takasuka and Satoh (2021), but it is not applicable to the same region (WP in their work). Currently we are not sure about the reason. After all, the region definitions are not exactly the same, and both works suffer from too few cases over the MC and WP. We have also discussed the differences between the roles of ER wave intrusion in MC initiation and in MC barrier effect at the end of section 4c.

Although the eastward propagations of MJO also show a diversity and the physical mechanism to explain it is still open (Suematsu and Miura 2022), the initiation mechanism has its own unique complexity since it concerns the formation of an intraseasonal disturbance from scratch, or from a weak and standing perturbation to a strong and propagating one (e.g., the MC scenario). Besides, there are various sources contributing to the initiation, including tropical atmospheric processes, delayed air–sea interactions, and extratropical origins. The current study explores the initiation mechanism through a composite procedure. Those significant composite results

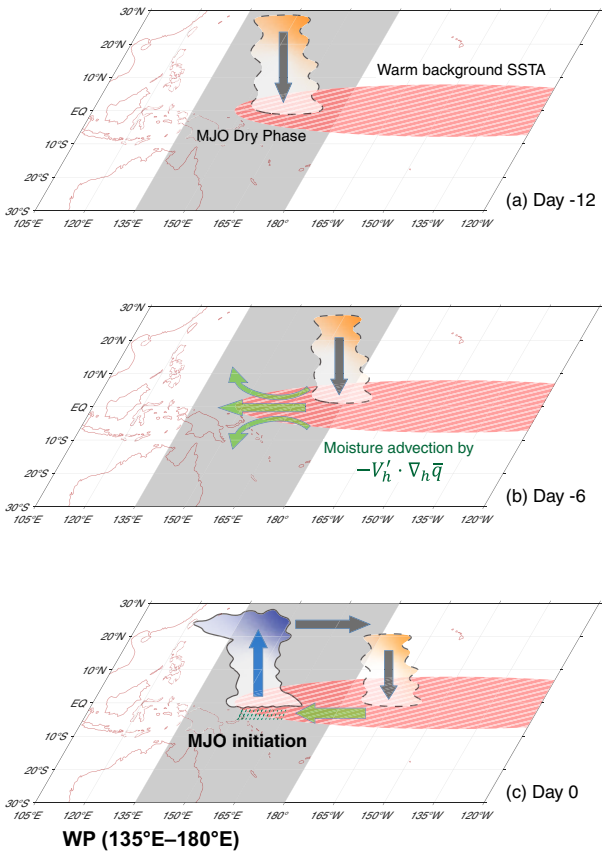

FIG. 17. A schematic diagram of MJO convection initiation over the WP region. The red shading with white stripes denotes the warm background SST anomaly. Other implications of the elements are as in Fig. 7.

suggest a list of candidate processes appropriate to most of the MJO initiations over a given region, helping us understanding how the dominant initiation mechanisms vary as a function of geographical location. However, it does not assume that there is a single mechanistic pathway. For instance, the downstream moisture advection, the delayed air–sea interaction, and the extratropical forcing may or may not work in concert in each individual case of IO initiation. It is also possible that some unimportant or infrequent processes are ignored due to limited sample size. Issues about how the initiation processes vary from case to case and what are their climatological relative contributions (e.g., Mei et al. 2015; Li et al. 2015; Feng and Li 2016) are beyond our scope, and should be addressed in the future, perhaps with a particular focus on the contrast between primary and successive events. In addition, Takasuka and Satoh (2021) showed that numerical experiments would be a useful tool in verifying the background modulation on favorable initiation regions, and should be adopted in the future work.

Acknowledgments. This work was jointly supported by NSFC Grant 42088101, NOAA NA18OAR4310298, and NSF AGS-2006553. This is SOEST Contribution Number 11571, IPRC Contribution Number 1576, and ESMC Number 388.

Data availability statement. The OLR and CMAP data are provided by the NOAA/OAR/ESRL PSL, Boulder, Colorado, from their website at https://psl.noaa.gov/. The ERA5 reanalysis data are available at Copernicus Climate Change Service Climate Data Store (CDS), https://cds.climate.copernicus.eu/#!/search?text=ERA5&type=dataset. The GHRSST Level 4 AVHRR_OI Global Blended Sea Surface Temperature Analysis (GDS2) data from NCEI, version 2.1. are available at https://podaac.jpl.nasa.gov/dataset/AVHRR_OI-NCEI-L4-GLOB-v2.1.

REFERENCES

Benedict, J. J., and D. A. Randall, 2007: Observed characteristics of the MJO relative to maximum rainfall. *J. Atmos. Sci.*, **64**, 2332–2354, https://doi.org/10.1175/JAS3968.1.

Benjamini, Y., and Y. Hochberg, 1995: Controlling the false discovery rate: A practical and powerful approach to multiple testing. *J. Roy. Stat. Soc.*, **57**, 289–300, https://doi.org/10.1111/j.2517-6161.1995.tb02031.x.

Bladé, I., and D. L. Hartmann, 1993: Tropical intraseasonal oscillations in a simple nonlinear model. *J. Atmos. Sci.*, **50**, 2922–2939, https://doi.org/10.1175/1520-0469(1993)050<2922:TIOIAS>2.0.CO;2.

Chen, G., 2021: Diversity of the global teleconnections associated with the Madden–Julian oscillation. *J. Climate*, **34**, 397–414, https://doi.org/10.1175/JCLI-D-20-0357.1.

——, and B. Wang, 2021: Diversity of the boreal summer intraseasonal oscillation. *J. Geophys. Res. Atmos.*, **126**, e2020JD034137, https://doi.org/10.1029/2020JD034137.

Chen, X., and F. Zhang, 2019: Relative roles of preconditioning moistening and global circumnavigating mode on the MJO convective initiation during DYNAMO. *Geophys. Res. Lett.*, **46**, 1079–1087, https://doi.org/10.1029/2018GL080987.

Chikira, M., 2014: Eastward-propagating intraseasonal oscillation represented by Chikira–Sugiyama cumulus parameterization. Part II: Understanding moisture variation under weak temperature gradient balance. *J. Atmos. Sci.*, **71**, 615–639, https://doi.org/10.1175/JAS-D-13-038.1.

DeMott, C. A., B. O. Wolding, E. D. Maloney, and D. A. Randall, 2018: Atmospheric mechanisms for MJO decay over the Maritime Continent. *J. Geophys. Res. Atmos.*, **123**, 5188–5204, https://doi.org/10.1029/2017JD026979.

Everitt, B. S., S. Landau, M. Leese, and D. Stahl, 2011: *Cluster Analysis*. 5th ed. John Wiley and Sons, 237 pp.

Feng, J., and T. Li, 2016: Initiation mechanisms for a successive MJO event and a primary MJO event during boreal winter of 2000-2001. *J. Trop. Meteor.*, **22**, 479–496, https://doi.org/10.16555/j.1006-8775.2016.04.004.

——, ——, and W. Zhu, 2015: Propagating and nonpropagating MJO events over Maritime Continent. *J. Climate*, **28**, 8430–8449, https://doi.org/10.1175/JCLI-D-15-0085.1.

Gill, A. E., 1980: Some simple solutions for heat-induced tropical circulation. *Quart. J. Roy. Meteor. Soc.*, **106**, 447–462, https://doi.org/10.1002/qj.49710644905.

Haertel, P., K. Straub, and A. Budsock, 2015: Transforming circumnavigating Kelvin waves that initiate and dissipate the Madden–Julian Oscillation. *Quart. J. Roy. Meteor. Soc.*, **141**, 1586–1602, https://doi.org/10.1002/qj.2461.

Hendon, H. H., 1988: A simple model of the 40–50 day oscillation. *J. Atmos. Sci.*, **45**, 569–584, https://doi.org/10.1175/1520-0469(1988)045<0569:ASMOTD>2.0.CO;2.

Hersbach, H., and Coauthors, 2020: The ERA5 global reanalysis. *Quart. J. Roy. Meteor. Soc.*, **146**, 1999–2049, https://doi.org/10.1002/qj.3803.

Hsu, H.-H., and M.-Y. Lee, 2005: Topographic effects on the eastward propagation and initiation of the Madden–Julian Oscillation. *J. Climate*, **18**, 795–809, https://doi.org/10.1175/JCLI-3292.1.

——, B. J. Hoskins, and F.-F. Jin, 1990: The 1985/86 intraseasonal oscillation and the role of the extratropics. *J. Atmos. Sci.*, **47**, 823–839, https://doi.org/10.1175/1520-0469(1990)047<0823:TIOATR>2.0.CO;2.

Hsu, P., and T. Li, 2012: Role of the boundary layer moisture asymmetry in causing the eastward propagation of the Madden–Julian Oscillation. *J. Climate*, **25**, 4914–4931, https://doi.org/10.1175/JCLI-D-11-00310.1.

Hu, Q., and D. A. Randall, 1994: Low-frequency oscillations in radiative-convective systems. *J. Atmos. Sci.*, **51**, 1089–1099, https://doi.org/10.1175/1520-0469(1994)051<1089:LFOIRC>2.0.CO;2.

Jiang, X.-A., and T. Li, 2005: Reinitiation of the boreal summer intraseasonal oscillation in the tropical Indian Ocean. *J. Climate*, **18**, 3777–3795, https://doi.org/10.1175/JCLI3516.1.

Kaufman, L., and P. J. Rousseeuw, 2005: *Finding Groups in Data: An Introduction to Cluster Analysis*. Wiley Series in Probability and Statistics, Vol. 603, John Wiley and Sons, 342 pp.

Kemball-Cook, S. R., and B. C. Weare, 2001: The onset of convection in the Madden–Julian oscillation. *J. Climate*, **14**, 780–793, https://doi.org/10.1175/1520-0442(2001)014<0780:TOOCIT>2.0.CO;2.

Kikuchi, K., and Y. N. Takayabu, 2003: Equatorial circumnavigation of moisture signal associated with the Madden-Julian oscillation (MJO) during boreal winter. *J. Meteor. Soc. Japan*, **81**, 851–869. https://doi.org/10.2151/jmsj.81.851.

Kiladis, G. N., and K. M. Weickmann, 1992: Circulation anomalies associated with tropical convection during northern winter. *Mon. Wea. Rev.*, **120**, 1900–1923, https://doi.org/10.1175/1520-0493(1992)120<1900:CAAWTC>2.0.CO;2.

——, J. Dias, K. H. Straub, M. C. Wheeler, S. N. Tulich, K. Kikuchi, K. M. Weickmann, and M. J. Ventrice, 2014: A comparison of OLR and circulation-based indices for tracking the MJO. *Mon. Wea. Rev.*, **142**, 1697–1715, https://doi.org/10.1175/MWR-D-13-00301.1.

Kim, D., J. Kug, and A. H. Sobel, 2014: Propagating versus nonpropagating Madden–Julian oscillation events. *J. Climate*, **27**, 111–125, https://doi.org/10.1175/JCLI-D-13-00084.1.

——, H. Kim, and M. I. Lee, 2017: Why does the MJO detour the Maritime Continent during austral summer? *Geophys. Res. Lett.*, **44**, 2579–2587, https://doi.org/10.1002/2017GL072643.

Knutson, T. R., and K. M. Weickmann, 1987: 30–60 day atmospheric oscillations: Composite life cycles of convection and circulation anomalies. *Mon. Wea. Rev.*, **115**, 1407–1436, https://doi.org/10.1175/1520-0493(1987)115<1407:DAOCLC>2.0.CO;2.

——, ——, and J. E. Kutzbach, 1986: Global-scale intraseasonal oscillations of outgoing longwave radiation and 250 mb zonal wind during Northern Hemisphere summer. *Mon. Wea. Rev.*, **114**, 605–623, https://doi.org/10.1175/1520-0493(1986)114<0605:GSIOOO>2.0.CO;2.

Kohyama, T., T. Suematsu, H. Miura, and D. Takasuka, 2021: A wall-like sharp downward branch of the Walker circulation above the western Indian Ocean. *J. Geophys. Res. Atmos.*, **126**, e2021JD034650, https://doi.org/10.1029/2021JD034650.

Lau, K.-M., and L. Peng, 1987: Origin of low-frequency (intraseasonal) oscillations in the tropical atmosphere. Part I: Basic theory. *J. Atmos. Sci.*, **44**, 950–972, https://doi.org/10.1175/1520-0469(1987)044<0950:OOLFOI>2.0.CO;2.

Li, T., 2014: Recent advance in understanding the dynamics of the Madden-Julian oscillation. *J. Meteor. Res.*, **28**, 1–33, https://doi.org/10.1007/s13351-014-3087-6.

——, Y. Zhang, E. Lu, and D. Wang, 2002: Relative role of dynamic and thermodynamic processes in the development of the Indian Ocean dipole: An OGCM diagnosis. *Geophys. Res. Lett.*, **29**, 2110, https://doi.org/10.1029/2002GL015789.

——, F. Tam, X. Fu, T. Zhou, and W. Zhu, 2008: Causes of the intraseasonal SST variability in the tropical Indian Ocean. *Atmos. Oceanic Sci. Lett.*, **1**, 18–23, https://doi.org/10.1080/16742834.2008.11446758.

——, C. Zhao, P. Hsu, and T. Nasuno, 2015: MJO initiation processes over the tropical Indian Ocean during DYNAMO/CINDY2011. *J. Climate*, **28**, 2121–2135, https://doi.org/10.1175/JCLI-D-14-00328.1.

——, L. Wang, M. Peng, B. Wang, C. Zhang, W. Lau, and H. -C. Kuo, 2018: A paper on the tropical intraseasonal oscillation published in 1963 in a Chinese journal. *Bull. Amer. Meteor. Soc.*, **99**, 1765–1779, https://doi.org/10.1175/BAMS-D-17-0216.1.

——, J. Ling, and P.-C. Hsu, 2020: Madden-Julian Oscillation: Its discovery, dynamics, and impact on East Asia. *J. Meteor. Res.*, **34**, 20–42, https://doi.org/10.1007/s13351-020-9153-3.

Liebmann, B., and C. A. Smith, 1996: Description of a complete (interpolated) outgoing longwave radiation dataset. *Bull. Amer. Meteor. Soc.*, **77**, 1275–1277, https://doi.org/10.1175/1520-0477-77.6.1274.

Madden, R. A., and P. R. Julian, 1971: Detection of a 40–50 day oscillation in the zonal wind in the tropical Pacific. *J. Atmos. Sci.*, **28**, 702–708, https://doi.org/10.1175/1520-0469(1971)028<0702:DOADOI>2.0.CO;2.

——, and ——, 1972: Description of global-scale circulation cells in the tropics with a 40–50 day period. *J. Atmos. Sci.*, **29**, 1109–1123, https://doi.org/10.1175/1520-0469(1972)029<1109:DOGSCC>2.0.CO;2.

——, and ——, 1994: Observations of the 40–50-day tropical oscillation—A review. *Mon. Wea. Rev.*, **122**, 814–837, https://doi.org/10.1175/1520-0493(1994)122<0814:OOTDTO>2.0.CO;2.

Maloney, E. D., and S. K. Esbensen, 2003: The amplification of east Pacific Madden–Julian oscillation convection and wind anomalies during June–November. *J. Climate*, **16**, 3482–3497, https://doi.org/10.1175/1520-0442(2003)016<3482:TAOEPM>2.0.CO;2.

——, and B. O. Wolding, 2015: Initiation of an intraseasonal oscillation in an aquaplanet general circulation model. *J. Adv. Model. Earth Syst.*, **7**, 1956–1976, https://doi.org/10.1002/2015MS000495.

Matsuno, T., 1966: Quasi-geostrophic motions in the equatorial area. *J. Meteor. Soc. Japan*, **44**, 25–43, https://doi.org/10.2151/jmsj1965.44.1_25.

Matthews, A. J., 2000: Propagation mechanisms for the Madden–Julian Oscillation. *Quart. J. Roy. Meteor. Soc.*, **126**, 2637–2651, https://doi.org/10.1002/qj.49712656902.

——, 2008: Primary and successive events in the Madden–Julian Oscillation. *Quart. J. Roy. Meteor. Soc.*, **134**, 439–453, https://doi.org/10.1002/qj.224.

——, and G. N. Kiladis, 1999: The tropical–extratropical interaction between high-frequency transients and the Madden–

Julian oscillation. *Mon. Wea. Rev.*, **127**, 661–677, https://doi.org/10.1175/1520-0493(1999)127<0661:TTEIBH>2.0.CO;2.

Mei, S., T. Li, and W. Chen, 2015: Three-type MJO initiation processes over the western equatorial Indian Ocean. *Adv. Atmos. Sci.*, **32**, 1208–1216, https://doi.org/10.1007/s00376-015-4201-0.

Milliff, R. F., and R. A. Madden, 1996: The existence and vertical structure of fast, eastward-moving disturbances in the equatorial troposphere. *J. Atmos. Sci.*, **53**, 586–597, https://doi.org/10.1175/1520-0469(1996)053<0586:TEAVSO>2.0.CO;2.

Nasuno, T., T. Li, and K. Kikuchi, 2015: Moistening processes before the convective initiation of Madden–Julian oscillation events during the CINDY2011/DYNAMO period. *Mon. Wea. Rev.*, **143**, 622–643, https://doi.org/10.1175/MWR-D-14-00132.1.

Pan, L.-L., and T. Li, 2008: Interactions between the tropical ISO and midlatitude low-frequency flow. *Climate Dyn.*, **31**, 375–388, https://doi.org/10.1007/s00382-007-0272-7.

Pokhrel, S., U. Dutta, H. Rahaman, H. Chaudhari, A. Hazra, S. K. Saha, and C. Veeranjaneyulu, 2020: Evaluation of different heat flux products over the tropical Indian Ocean. *Earth Space Sci.*, **7**, e2019EA000988, https://doi.org/10.1029/2019EA000988.

Powell, S. W., 2016: Updraft buoyancy within and moistening by cumulonimbi prior to MJO convective onset in a regional model. *J. Atmos. Sci.*, **73**, 2913–2934, https://doi.org/10.1175/JAS-D-15-0326.1.

——, and R. A. Houze Jr., 2015: Effect of dry large-scale vertical motions on initial MJO convective onset. *J. Geophys. Res. Atmos.*, **120**, 4783–4805, https://doi.org/10.1002/2014JD022961.

Ray, P., and T. Li, 2013: Relative roles of circumnavigating waves and extratropics on the MJO and its relationship with the mean state. *J. Atmos. Sci.*, **70**, 876–893, https://doi.org/10.1175/JAS-D-12-0153.1.

——, C. Zhang, J. Dudhia, and S. S. Chen, 2009: A numerical case study on the initiation of the Madden–Julian oscillation. *J. Atmos. Sci.*, **66**, 310–331, https://doi.org/10.1175/2008JAS2701.1.

Reynolds, R. W., T. M. Smith, C. Liu, D. B. Chelton, K. S. Casey, and M. G. Schlax, 2007: Daily high-resolution-blended analyses for sea surface temperature. *J. Climate*, **20**, 5473–5496, https://doi.org/10.1175/2007JCLI1824.1.

Roundy, P. E., 2014: Some aspects of Western Hemisphere circulation and the Madden–Julian oscillation. *J. Atmos. Sci.*, **71**, 2027–2039, https://doi.org/10.1175/JAS-D-13-0210.1.

——, and W. M. Frank, 2004: Effects of low-frequency wave interactions on intraseasonal oscillations. *J. Atmos. Sci.*, **61**, 3025–3040, https://doi.org/10.1175/JAS-3348.1.

Rydbeck, A. V., and T. G. Jensen, 2017: Oceanic impetus for convective onset of the Madden–Julian oscillation in the western Indian Ocean. *J. Climate*, **30**, 4299–4316, https://doi.org/10.1175/JCLI-D-16-0595.1.

Saji, N. H., S.-P. Xie, and C.-Y. Tam, 2006: Satellite observations of intense intraseasonal cooling events in the tropical south Indian Ocean. *Geophys. Res. Lett.*, **33**, L14704, https://doi.org/10.1029/2006GL026525.

Seo, K.-H., and K.-Y. Kim, 2003: Propagation and initiation mechanisms of the Madden-Julian oscillation. *J. Geophys. Res. Atmos.*, **108**, 4384, https://doi.org/10.1029/2002JD002876.

Sobel, A. H., and D. Kim, 2012: The MJO-Kelvin wave transition. *Geophys. Res. Lett.*, **39**, L20808, https://doi.org/10.1029/2012GL053380.

——, S. Wang, and D. Kim, 2014: Moist static energy budget of the MJO during DYNAMO. *J. Atmos. Sci.*, **71**, 4276–4291, https://doi.org/10.1175/JAS-D-14-0052.1.

Straub, K. H., 2013: MJO initiation in the real-time multivariate MJO index. *J. Climate*, **26**, 1130–1151, https://doi.org/10.1175/JCLI-D-12-00074.1.

Suematsu, T., and H. Miura, 2018: Zonal SST difference as a potential environmental factor supporting the longevity of the Madden–Julian oscillation. *J. Climate*, **31**, 7549–7564, https://doi.org/10.1175/JCLI-D-17-0822.1.

——, and ——, 2022: Changes in the eastward movement speed of the Madden–Julian oscillation with fluctuation in the Walker circulation. *J. Climate*, **35**, 211–225, https://doi.org/10.1175/JCLI-D-21-0269.1.

Takasuka, D., and M. Satoh, 2021: Diversity of the Madden–Julian oscillation: Initiation region modulated by the interaction between the intraseasonal and interannual variabilities. *J. Climate*, **34**, 2297–2318, https://doi.org/10.1175/JCLI-D-20-0688.1.

——, T. Kohyama, H. Miura, and T. Suematsu, 2021: MJO initiation triggered by amplification of upper-tropospheric dry mixed Rossby-gravity waves. *Geophys. Res. Lett.*, **48**, e2021GL094239, https://doi.org/10.1029/2021GL094239.

Vitart, F., and Coauthors, 2017: The Subseasonal to Seasonal (S2S) Prediction project database. *Bull. Amer. Meteor. Soc.*, **98**, 163–173, https://doi.org/10.1175/BAMS-D-16-0017.1.

Waliser, D. E., R. Murtugudde, and L. E. Lucas, 2003: Indo-Pacific Ocean response to atmospheric intraseasonal variability: 1. Austral summer and the Madden-Julian Oscillation. *J. Geophys. Res.*, **108**, 3160, https://doi.org/10.1029/2002JC001620.

——, ——, and ——, 2004: Indo-Pacific Ocean response to atmospheric intraseasonal variability: 2. Boreal summer and the Intraseasonal Oscillation. *J. Geophys. Res.*, **109**, C03030, https://doi.org/10.1029/2003JC002002.

——, and Coauthors, 2012: The "Year" of Tropical Convection (May 2008–April 2010): Climate variability and weather highlights. *Bull. Amer. Meteor. Soc.*, **93**, 1189–1218, https://doi.org/10.1175/2011BAMS3095.1.

Wang, B., 1988: Dynamics of tropical low-frequency waves: An analysis of the moist Kelvin wave. *J. Atmos. Sci.*, **45**, 2051–2065, https://doi.org/10.1175/1520-0469(1988)045<2051:DOTLFW>2.0.CO;2.

——, and H. Rui, 1990: Synoptic climatology of transient tropical intraseasonal convection anomalies: 1975–1985. *Meteor. Atmos. Phys.*, **44**, 43–61, https://doi.org/10.1007/BF01026810.

——, and T. Li, 1994: Convective interaction with boundary layer dynamics in the development of a tropical intraseasonal system. *J. Atmos. Sci.*, **51**, 1386–1400, https://doi.org/10.1175/1520-0469(1994)051<1386:CIWBLD>2.0.CO;2.

——, and X. Xie, 1996: Low-frequency equatorial waves in vertically sheared zonal flow. Part I: Stable waves. *J. Atmos. Sci.*, **53**, 449–467, https://doi.org/10.1175/1520-0469(1996)053<0449:LFEWIV>2.0.CO;2.

——, and G. Chen, 2017: A general theoretical framework for understanding essential dynamics of Madden–Julian oscillation. *Climate Dyn.*, **49**, 2309–2328, https://doi.org/10.1007/s00382-016-3448-1.

——, F. Liu, and G. Chen, 2016: A trio-interaction theory for Madden–Julian oscillation. *Geosci. Lett.*, **3**, 34, https://doi.org/10.1186/s40562-016-0066-z.

——, G. Chen, and F. Liu, 2019: Diversity of the Madden-Julian Oscillation. *Sci. Adv.*, **5**, eaax0220, https://doi.org/10.1126/sciadv.aax0220.

Wang, H., F. Liu, B. Wang, G. Chen, and W. Dong, 2021: Diversity of intraseasonal oscillation over the western North Pacific. *Climate Dyn.*, **57**, 1881–1893, https://doi.org/10.1007/s00382-021-05780-2.

Wang, L., T. Li, E. Maloney, and B. Wang, 2017: Fundamental causes of propagating and nonpropagating MJOs in MJOTF/GASS models. *J. Climate*, **30**, 3743–3769, https://doi.org/10.1175/JCLI-D-16-0765.1.

Wang, T., and T. Li, 2021: Factors controlling the diversities of MJO propagation and intensity. *J. Climate*, **34**, 6549–6563, https://doi.org/10.1175/JCLI-D-20-0859.1.

——, X.-Q. Yang, J. Fang, X. Sun, and X. Ren, 2018: Role of air–sea interaction in the 30–60-day boreal summer intraseasonal oscillation over the western North Pacific. *J. Climate*, **31**, 1653–1680, https://doi.org/10.1175/JCLI-D-17-0109.1.

Wierzchon, S., and M. Klopotek, 2018: *Modern Algorithms of Cluster Analysis*. 1st ed. Springer, 441 pp.

Wilks, D. S., 2006: On "field significance" and the false discovery rate. *J. Appl. Meteor. Climatol.*, **45**, 1181–1189, https://doi.org/10.1175/JAM2404.1.

——, 2016: "The stippling shows statistically significant grid points": How research results are routinely overstated and overinterpreted, and what to do about it. *Bull. Amer. Meteor. Soc.*, **97**, 2263–2273, https://doi.org/10.1175/BAMS-D-15-00267.1.

Wolding, B. O., and E. D. Maloney, 2015: Objective diagnostics and the Madden–Julian oscillation. Part II: Application to moist static energy and moisture budgets. *J. Climate*, **28**, 7786–7808, https://doi.org/10.1175/JCLI-D-14-00689.1.

Wu, B., T. Zhou, and T. Li, 2009: Contrast of rainfall–SST relationships in the western North Pacific between the ENSO-developing and ENSO-decaying summers. *J. Climate*, **22**, 4398–4405, https://doi.org/10.1175/2009JCLI2648.1.

Xie, P., and P. A. Arkin, 1997: Global precipitation: A 17-year monthly analysis based on gauge observations, satellite estimates, and numerical model outputs. *Bull. Amer. Meteor. Soc.*, **78**, 2539–2558, https://doi.org/10.1175/1520-0477(1997)078<2539:GPAYMA>2.0.CO;2.

Xie, X., and B. Wang, 1996: Low-frequency equatorial waves in vertically sheared zonal flow. Part II: Unstable waves. *J. Atmos. Sci.*, **53**, 3589–3605, https://doi.org/10.1175/1520-0469(1996)053<3589:LFEWIV>2.0.CO;2.

Xie, Y., S. Chen, Y. Zhang, and Y. Huang, 1963: A preliminarily statistic and synoptic study about the basic currents over southeastern Asia and the initiation of typhoon (in Chinese). *Acta Meteor. Sin.*, **33**, 206–217, https://doi.org/10.11676/qxxb1963.020.

Yanai, M., S. Esbensen, and J. Chu, 1973: Determination of bulk properties of tropical cloud clusters from large-scale heat and moisture budgets. *J. Atmos. Sci.*, **30**, 611–627, https://doi.org/10.1175/1520-0469(1973)030<0611:DOBPOT>2.0.CO;2.

Yu, L., 2007: Global variations in oceanic evaporation (1958–2005): The role of the changing wind speed. *J. Climate*, **20**, 5376–5390, https://doi.org/10.1175/2007JCLI1714.1.

——, X. Jin, and R. A. Weller, 2008: Multidecade global flux datasets from the Objectively Analyzed Air-sea Fluxes (OAFlux) project: Latent and sensible heat fluxes, ocean evaporation, and related surface meteorological variables. OAFlux Project Tech. Rep. OA-2008-01, Woods Hole Oceanographic Institution, 64 pp.

Zhang, C., 2005: Madden–Julian Oscillation. *Rev. Geophys.*, **43**, RG2003, https://doi.org/10.1029/2004RG000158.

——, 2013: Madden–Julian oscillation: Bridging weather and climate. *Bull. Amer. Meteor. Soc.*, **94**, 1849–1870, https://doi.org/10.1175/BAMS-D-12-00026.1.

——, and H. H. Hendon, 1997: Propagating and standing components of the intraseasonal oscillationin tropical convection. *J. Atmos. Sci.*, **54**, 741–752, https://doi.org/10.1175/1520-0469(1997)054<0741:PASCOT>2.0.CO;2.

——, and J. Ling, 2017: Barrier effect of the Indo-Pacific Maritime Continent on the MJO: Perspectives from tracking MJO precipitation. *J. Climate*, **30**, 3439–3459, https://doi.org/10.1175/JCLI-D-16-0614.1.

Zhao, C., T. Li, and T. Zhou, 2013: Precursor signals and processes associated with MJO initiation over the tropical Indian Ocean. *J. Climate*, **26**, 291–307, https://doi.org/10.1175/JCLI-D-12-00113.1.